

Synaptotagmin-11 deficiency mediates schizophrenia-like behaviors in mice via dopamine over-transmission

Received: 27 March 2024

Accepted: 15 November 2024

Published online: 04 December 2024

 Check for updates

Yang Chen^{1,10}, Yuhao Gu^{1,10}, Bianbian Wang^{1,10}, Anqi Wei^{1,10}, Nan Dong¹, Yong Jiang², Xiaoying Liu^{1,3,4}, Li Zhu⁵, Feng Zhu⁶, Tao Tan⁷, Zexin Jing¹, Fenghan Mao¹, Yichi Zhang¹, Jingyu Yao¹, Yuxin Yang^{1,4}, Hongyan Wang⁴, Hao Wu¹, Hua Li¹, Chaowen Zheng¹, Xueting Duan¹, Jingxiao Huo¹, Xuanang Wu¹, Shaoqin Hu¹, Anran Zhao¹, Ziyang Li¹, Xu Cheng³, Yuhao Qin³, Qian Song¹, Shuqin Zhan¹, Qiumin Qu⁸, Fanglin Guan⁵✉, Huadong Xu¹✉, Xinjiang Kang^{2,3,4}✉ & Changhe Wang^{1,2,3,9}✉

Schizophrenia is a severe neuropsychiatric disease, but the initiation mechanisms are unclear. Although antipsychotics are effective against positive symptoms, therapeutic interventions for negative symptoms are limited due to the lack of pathophysiological mechanisms. Here we identify synaptotagmin-11 (Syt11) as a potential genetic risk factor and dopamine over-transmission as a mechanism in the development of schizophrenia. Syt11 expression is reduced in individuals with schizophrenia but restored following the treatment with antipsychotics. Syt11 deficiency in dopamine neurons in early adolescence, but not in adults, leads to persistent social deficits and other schizophrenia-like behaviors by mediating dopamine over-transmission in mice. Accordingly, dopamine neuron over-excitation before late adolescence induces persistent schizophrenia-associated behavioral deficits, along with the structural and functional alternations in the mPFC. Notably, local intervention of D2R with clinical drugs presynaptically or postsynaptically exhibits both acute and long-lasting therapeutic effects on social deficits in schizophrenia mice models. These findings not only define Syt11 as a risk factor and DA over-transmission as a potential risk factor initiating schizophrenia, but also propose two D2R-targeting strategies for the comprehensive and long-term recovery of schizophrenia-associated social withdrawal.

Schizophrenia is a chronic and disabling psychiatric disorder with a prevalence of 1% worldwide. This disease is characterized by the manifestation of positive symptoms such as delusions and hallucinations, negative symptoms such as social withdrawal and loss of motivation, and cognitive dysfunction^{1–3}. The onset of schizophrenia is typically characterized by social withdrawal and cognitive decline, which usually begins in early adolescence and precedes the psychotic episode by

several years. While antipsychotic medications are effective in treating positive symptoms in ~70% of patients^{4–6}, they fail to improve negative symptoms and cognitive impairments, which are considered as core features of the disorder throughout the lifetime⁷. Despite recent advancements in understanding the etiology of schizophrenia, the underlying pathophysiological mechanisms responsible for negative symptoms, particularly social withdrawal, remain largely unknown.

A full list of affiliations appears at the end of the paper. ✉ e-mail: fanglingguan@163.com; hdxu@pku.edu.cn; kxj335@163.com; changhewang@xjtu.edu.cn

Converging evidence suggests that aberrant dopamine (DA) transmission is associated with the positive psychotic symptoms of schizophrenia^{2,8–13}. However, the concept of hyperactive DA transmission has been challenged due to inconsistent clinical observations^{4,14–17} and is proposed to be downstream of hyperactive glutamatergic projections or the consequence of excitatory-inhibitory imbalance of synaptic inputs^{4,8,15,18}. Although most currently-licensed antipsychotic agents (e.g., chlorpromazine, haloperidol, clozapine, phenothiazine, and butyrophenone) are suggested to alleviate positive symptoms mainly through antagonizing D2 receptors (D2Rs)^{2,8}, there is little direct evidence (real time recordings) demonstrating aberrant DA transmission in schizophrenia. The role of DA dysfunction in the onset of schizophrenia remains a topic of debate in this field.

Based on the inability of D2R antagonists in treating negative symptoms, the ‘dual dysregulation’ hypothesis has been proposed as a reformulation of the DA hypothesis^{15,19}. According to this hypothesis, excess striatal DA transmission leads to positive symptoms of schizophrenia, while cortical hypodopaminergic function is implicated in the negative and cognitive aspects^{15,17,19}. However, the evidence for extrastriatal DA deficits primarily relies on the indirect measurements of DA levels in response to amphetamine administration or depletion paradigm in preclinical and postmortem observations^{14,17}. The causal relationship between DA deficiency and negative symptoms is largely speculative and has not been adequately assessed to date. Thus, it remains unclear whether and how extrastriatal DA transmission contributes to the manifestation of negative and cognitive symptoms in schizophrenia.

Large-scale genetic studies have identified numerous genes associated with schizophrenia, but only few of them have been shown to be sufficient to independently trigger the onset of schizophrenia^{20–22}. Thus, ideal genetic mouse models for schizophrenia study are still lacking. Recent studies have identified *SYT11* as a candidate gene implicated in both familial and sporadic schizophrenia susceptibility^{23,24}. Synaptotagmins (Syts) are primary Ca²⁺ sensors that mediate SNARE-dependent vesicle fusion during neurotransmission²⁵. We have recently found that Syt11, a non-Ca²⁺-binding Syt²⁶, acts as a constitutive brake of endocytosis in neurons^{27–29}, while Syt11 accumulation mediates the neurodegenerative changes in DA neurons, contributing to the pathogenesis of Parkinson’s disease by inhibiting vesicle recycling and DA release³⁰. However, it remains unknown whether and how Syt11 dysfunction leads to neurodevelopmental deficits and the pathogenesis of schizophrenia in mice.

In this study, we have identified Syt11 as a potential risk factor for schizophrenia, established plasma Syt11 as a biomarker for diagnosing schizophrenia, and developed Syt11 conditional knockout (cKO) mouse as a genetic mouse model for schizophrenia study. Importantly, our findings elucidate a role of DA over-transmission before late adolescence in the initiation of schizophrenia, particularly in relation to negative symptoms. Local administration of a D2R agonist in the ventral tegmental area (VTA, inhibiting presynaptic DA release) or an antagonist in the medial prefrontal cortex (mPFC, stimulating postsynaptic cortical neurons) during late adolescence yields similar long-lasting therapeutic effects on schizophrenia-like behavioral changes. Altogether, this work not only defines Syt11 as a potential risk factor and DA over-transmission as a neural mechanism initiating the pathogenesis of schizophrenia but also unveils a time window and a couple of D2R-targeting strategies for potential clinical treatment of schizophrenia.

Results

Syt11 deficiency is linked to schizophrenia

To investigate the potential association between Syt11 expression and schizophrenia, we analyzed Syt11 expression in three datasets of human brain tissues: the Lieber Institute for Brain Development (LIBD), the CommonMind Consortium (CMC), and the Human Brain

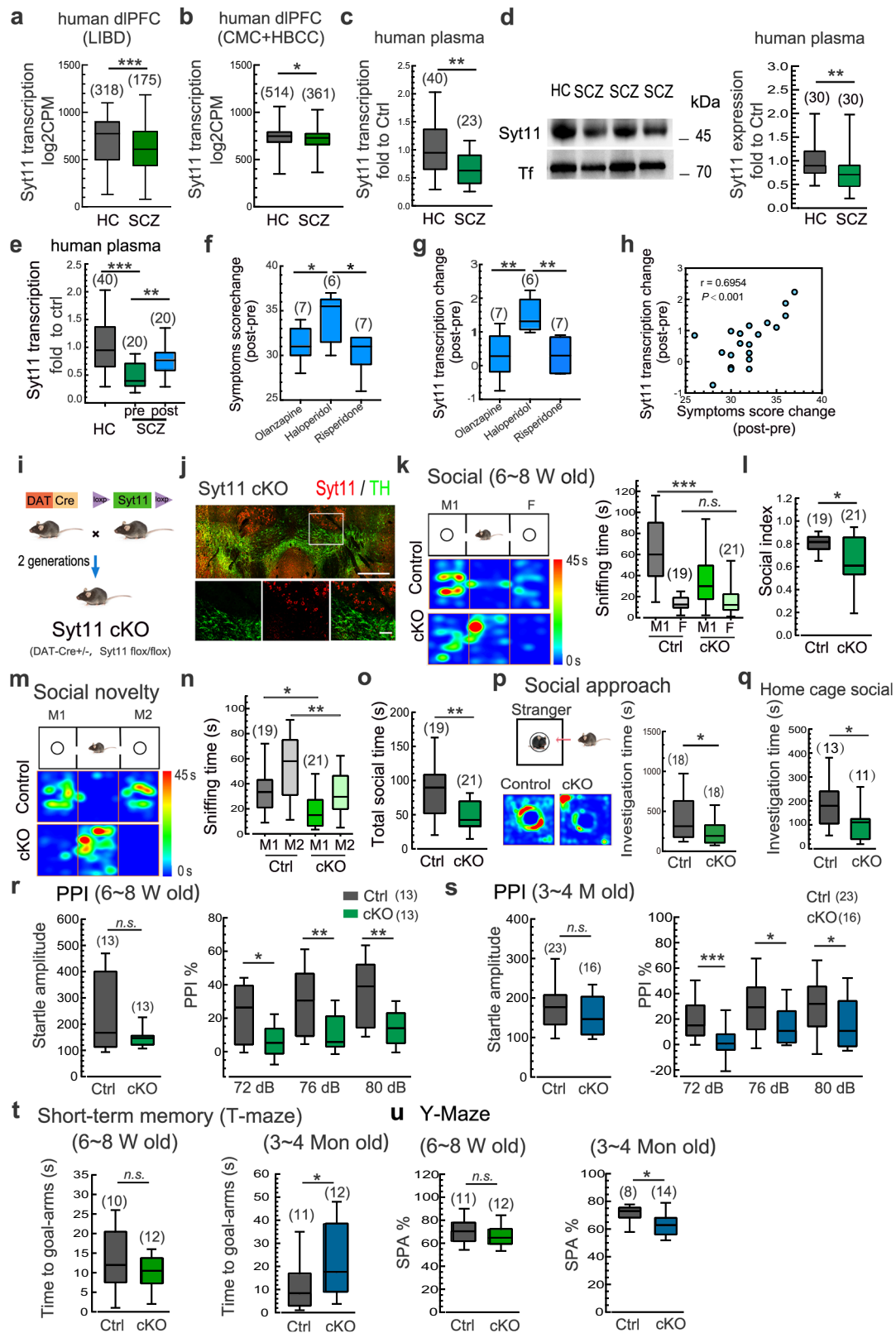
Collection Core (HBCC). These datasets included mRNA transcription profiles from the dorsolateral prefrontal cortex (dlPFC) of postmortem brains from both schizophrenia patients and healthy controls. To minimize site-specific technical variations, the CMC and HBCC datasets, which underwent RNA extraction and data generation at a single facility, were combined³¹. Our analysis revealed a significant reduction in Syt11 expression in prefrontal cortex tissues of schizophrenia patients (Fig. 1a, b). This finding was further confirmed by qPCR and Western blot analyses, which showed a significant decrease in both Syt11 transcription and protein expression in the plasma of schizophrenia patients in two independent case-control samples (Fig. 1c, d). Specifically, ~50% of schizophrenia patients showed a clear reduction of Syt11 expression in the plasma (by setting the threshold at the 90th percentile of the highest value in the healthy control group), with an area under the curve ratio (AUC) of 0.737 in the receiver operating characteristic (ROC) curve (Supplementary information, Fig. S1). These results not only identify Syt11 deficiency as a potential risk factor for the pathogenesis of schizophrenia, but also define plasma Syt11 as a biomarker for the clinical diagnosis of schizophrenia.

To validate the close association between Syt11 expression and schizophrenia, we next examined Syt11 expression in plasma samples collected from healthy individuals and schizophrenia patients before and after antipsychotic treatment. We found that the decreased expression of Syt11 in the plasma of schizophrenia patients was restored after the antipsychotic treatment with olanzapine, haloperidol, or risperidone (Fig. 1e). Specifically, patients who received the haloperidol treatment showed the most substantial changes in symptom scores when compared to those treated with olanzapine or risperidone, and this was correlated with the highest restoration of Syt11 expression in the haloperidol-treated patients (Fig. 1f, g). Importantly, Pearson’s correlation analysis demonstrated a positive correlation between the overall changes in schizophrenia symptom scores and the changes in Syt11 expression after antipsychotic treatment (Fig. 1h), suggesting that the rescue of Syt11 deficiency in schizophrenia patients is closely associated with the therapeutic effects of antipsychotic medications. Collectively, these findings from human samples and clinical treatment demonstrate the close association between Syt11 deficiency and schizophrenia.

DA neuron-restricted knockout of Syt11 leads to schizophrenia-like behaviors

To investigate the potential role of *SYT11* deficiency in initiating the pathogenesis of schizophrenia, we generated DA neuron-restricted Syt11 cKO mice by crossing homozygous floxed Syt11-null mice with DAT-driven Cre recombinase (DAT-Cre) transgenic mice (Fig. 1i), as previously described³⁰. Immunostaining for tyrosine hydroxylase (TH) confirmed the specific loss of Syt11 in midbrain DA neurons (Fig. 1j). The three-chamber social interaction test was employed to assess the social disability, a prominent negative symptom in schizophrenia, in young (6–8 weeks old) male Syt11-cKO mice (Fig. 1k). As expected, control mice (DAT-Cre) spent more time interacting with a stranger mouse (M1) than a fake mouse (F) (Fig. 1k). In contrast, Syt11-cKO mice showed reduced sniffing time with the M1 mouse, while their interaction with the F mouse remained unchanged, resulting in the decreased social preference index (Fig. 1k, l), suggesting impaired social preference upon Syt11 deficiency in DA neurons. Similarly, in the social novelty test, Syt11-cKO mice showed the reduced social preference for a new stranger mouse (M2) over a familiar one, in contrast to control mice (Fig. 1m, n). Importantly, the total sniffing time with both M1 and M2 mice decreased greatly in Syt11-cKO mice (Fig. 1o), confirming the impaired social activity in the absence of Syt11 in DA neurons.

Furthermore, we applied the social approach test to further evaluate the behavioral deficits in young Syt11-cKO mice (Fig. 1p). Compared to controls, Syt11-cKO mice spent significantly less time approaching and interacting with a caged stranger mouse (Fig. 1p). The



home-cage social test also revealed reduced social interaction of Syt11-cKO mice with a stranger intruder mouse (Fig. 1q), confirming that the DA neuron-restricted KO of Syt11 is sufficient to induce social deficits at early ages.

To examine whether these social deficits persist into adulthood, we conducted the same social behavioral tests with adult (3 months old) male Syt11-cKO mice. These mice also showed reduced sniffing

time with the M1 mouse and thus a decreased social preference index (Supplementary information, Fig. S2a-c). Similarly, cKO mice performed worse than controls in the social novelty test (Supplementary information, Fig. S2d-f). Similar social deficits were observed in Syt11 cKO mice at 1 year old (Supplementary information, Fig. S2i,j), indicating the long-lasting social withdrawal in the absence of Syt11. Additionally, adult cKO mice also showed decreased social interaction

Fig. 1 | Syt11 deficiency in dopamine neurons leads to schizophrenia-like behaviors. **a, b** Transcript expression levels of Syt11 in the dlPFC of postmortem brains from schizophrenia (SCZ) patients *vs* healthy controls (HC). RNA-sequencing data set were obtained from the Lieber Institute for Brain Development (LIBD), the CommonMind Consortium (CMC), and the Human Brain Collection Core (HBCC). The CMC and HBCC data sets were performed at a single facility with similar processes and thus combined to minimize site-specific sources of technical variation. **c** Transcript expression levels of Syt11 in peripheral blood from SCZ patients *vs* HC. **d** Representative western blots and expression levels of Syt11 in plasma from SCZ patients *vs* HC. **e** Transcript expression levels of Syt11 in peripheral blood from HC and SCZ patients before (SCZ-pre) and after (SCZ-post) antipsychotic treatment. **f** Changes in SCZ symptoms scores of SCZ patients after treatment with olanzapine, haloperidol, or risperidone. **g** Transcript expression changes of Syt11 in peripheral blood from SCZ patients after treatment with olanzapine, haloperidol, or risperidone. **h** Pearson correlation analysis between changes in Syt11 expression and changes in SCZ symptom scores after antipsychotic treatment as in (e-g). **i** Schematic of the generation of DA neuron-restricted Syt11 conditional knockout (cKO) mice. **j** Representative micrograph showing the immunostaining of Syt11 (red) and TH (green) in a VTA-containing slice (enlarged insets in the lower panel). Scale bars: 500 μ m (upper), 100 μ m (lower). Data from 3 mice. **k, l** Schematic, representative heat maps, and statistics of the three-chamber social interaction test

of juvenile (6–8 weeks) Syt11-cKO or DAT-Cre (Ctrl) mice. M1, a novel mouse; F, fake toy mouse. Sniffing time and social index of Syt11-cKO *vs* control mice were used for analysis. **m** Schematic and representative heat maps of the three-chamber social novelty test of juvenile Syt11-cKO *vs* control mice. M1, familiar mouse (the former novel mouse in **k** and **l**); M2, new comer novel mouse. **n, o** Statistics of sniffing time (with M1 or M2) and total social time (sniffing with M1 and M2) of Syt11-cKO *vs* control mice. **p** Left, schematic and representative heat maps of the social approach test. Right, statistics of sniffing time with a caged novel mouse of Syt11-cKO *vs* control mice (6–8 weeks). **q** Statistics of sniffing time with an intruder mouse of Syt11-cKO *vs* control mice (6–8 weeks) in the home-cage social test. **r, s** Statistics of startle responses and pre-pulse inhibition (PPI) of juvenile (6–8 weeks) and adult (3–4 months) Syt11-cKO mice *vs* control mice. **t** Statistics of short-term memory (T-maze) of juvenile and adult Syt11-cKO mice *vs* control mice. **u** Statistics of the spontaneous alternation Y-maze test of juvenile and adult Syt11-cKO mice *vs* control mice. Data are shown as box-and-whisker plots, with the median represented by the central line inside each box, the 25th and 75th percentiles represented by the edges of the box, and the whiskers extending to the most extreme data points. Two-tailed Mann-Whitney test for (a-d, l, o-q, r-u), Pearson correlation analysis for (h), one-way ANOVA for (f, g), or Ordinary two-way ANOVA followed by Bonferroni's multiple comparisons for (e, k, n), * $P < 0.05$, ** $P < 0.01$, *** $P < 0.001$, n.s. no significant difference. Source data are provided as a Source Data file.

time with the stimulus mouse in the social approach test (Supplementary information, Fig. S2g). Consistent with this, the social interaction time of adult Syt11-cKO mice with the stranger intruder mouse was shorter than that of controls (Supplementary information, Fig. S2h). Together, these results suggest an early-onset and enduring social withdrawal phenotype in DA neuron-restricted Syt11-cKO mice.

To further confirm the association of social withdrawal in Syt11-cKO mice with schizophrenia, we carried out a series of behavior analyses to examine other schizophrenia-related symptoms. In the locomotion test, Syt11-cKO mice showed the increased total travel distance with intact travel speed at adolescence (Supplementary information, Fig. S2k, l), indicating locomotion hyperactivity, which corresponds to the psychomotor agitation observed in schizophrenia patients. Furthermore, both adolescent and adult Syt11-cKO mice exhibited aberrant prepulse inhibition (PPI) of the acoustic startle response (Fig. 1r, s), a well-defined hallmark of sensorimotor gating dysfunction manifested in early adulthood in patients with schizophrenia. As a control, the intact startle amplitude indicated normal gross auditory and motor ability in Syt11-cKO mice (Fig. 1r, s). Although Syt11-cKO mice did not show clear impairments in the T-maze test during adolescence, adult cKO mice spent more time turning into the goal arm (Fig. 1t), suggesting deficits in short-term working memory upon Syt11 deficiency in DA neurons. In addition, the adult Syt11-cKO mice also performed poorly in a spontaneous alternation Y-maze test (Fig. 1u), consistent with the cognitive dysfunction observed in patients with schizophrenia from early adulthood. In contrast, the cKO mice did not show enhanced marble-burying behavior (Supplementary information, Fig. S2m) or excessive self-grooming in the open field test (Supplementary information, Fig. S2n), suggesting the absence of repetitive behaviors associated with autism³². Overall, these results demonstrate a role of Syt11 deficiency in DA neurons in mediating the pathogenesis of schizophrenia and provide a mouse model for schizophrenia study, particularly that related to social withdrawal and other negative symptoms.

Syt11 deficiency in early adolescence mediates social deficits

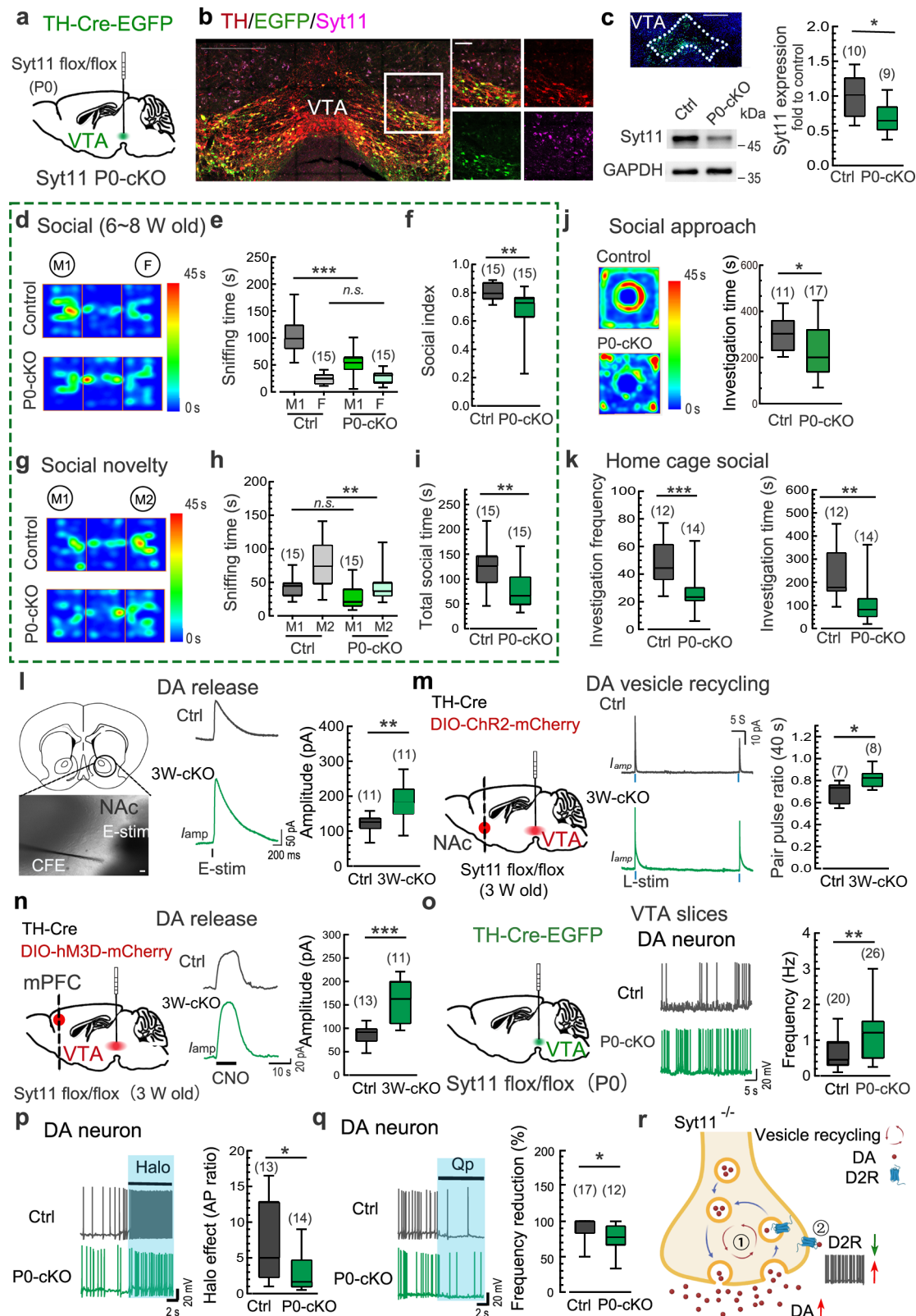
We aimed to investigate whether there is a sensitive time-window during which Syt11 deficiency leads to social deficits. To address this issue, we generated DA neuron-restricted knockout of Syt11 during early adolescence and adulthood, respectively. To generate DA neuron-restricted knockout of Syt11 at early adolescence, we stereotaxically injected a TH-Cre expressing AAV9 virus into the VTA of homozygous floxed Syt11-null mice on postnatal day 0–1 (P0, Fig. 2a). Immunostaining confirmed the absence of Syt11 in virus-infected DA

neurons (GFP-positive) in the VTA 6 weeks after virus injection (Fig. 2b; Supplementary information, Fig. S3a, b), and Western blot analysis validated the decreased expression of Syt11 in the ventral midbrain (Fig. 2c). Notably, DA neuron-restricted KO of Syt11 since P0 (P0-cKO) exhibited decreased sniffing time with M1 mice and a reduced social index in the three-chamber social interaction test during 6–8 weeks of age (Fig. 2d-f). Similarly, these Syt11 P0-cKO mice also showed decreased social preference for the stranger M2 mouse and reduced total social time with both mice compared with controls (Fig. 2g-i). In addition, Syt11 P0-cKO mice showed reduced social interaction with a caged stranger mouse in the social approach test (Fig. 2j) and the stranger intruder mouse in the home-cage social test (Fig. 2k). These findings indicate that the absence of Syt11 at an early age can mediate impairments in social ability. Importantly, adult Syt11 P0-cKO mice also showed impaired social behaviors in the three-chamber social test, social novelty test, and social approach test (Supplementary information, Fig. S3), suggesting that Syt11 deficiency since P0 is associated with ongoing social deficits.

To test whether Syt11 knockout in adult mice also results in social deficits, we generated Syt11 adult-cKO mice by injecting TH-Cre virus into the VTA of adult (3–4 months) Syt11-flox mice (Supplementary information, Figs. S4). Although Syt11-cKO led to increased DA release in the nucleus accumbens (NAc, Supplementary information, Fig. S5a) as revealed by electrochemical amperometric recordings, these mice spent similar amounts of time interacting with the M1 mouse and thus showed an unchanged social index in the three-chamber social interaction test (Supplementary information, Fig. S5b-d). In addition, the social preference for the M2 mouse and the total social time with both mice remained intact in adult-cKO mice compared with controls (Supplementary information, Fig. S5e-g). Syt11 adult-cKO mice also showed similar social interaction time with the caged stranger mouse in the social approach test (Supplementary information, Fig. S5h) and the stranger intruder mouse in the home-cage social test (Supplementary information, Fig. S5i). Collectively, these results demonstrate that Syt11 adult-cKO mice exhibit normal social behaviors, suggesting that there is a sensitive time-window before adult for Syt11 deficiency-mediated schizophrenia-like social deficits, further supporting the persistence of social deficits when Syt11 deficiency occurs at earlier ages, and implying a potential role of Syt11 in neural development.

Syt11 deficiency leads to DA over-transmission via the accelerated vesicle recycling and off-membrane trafficking of D2Rs

Our previous studies have shown that Syt11 serves as a clamp for endocytosis and thus inhibits vesicle replenishment and DA release,



while Syt11 cKO in midbrain DA neurons leads to excessive DA release in the striatum^{27,29,30}. Here, we further investigated whether Syt11 cKO in VTA^{DA} neurons leads to social deficits *via* DA over-transmission. To examine this, we applied amperometric recordings with electrochemical carbon fiber electrodes (CFEs) in the NAC and the medial prefrontal cortex (mPFC), which are DA neuron-projecting regions involved in social behaviors. Consistent with previous reports^{30,33}, local

electrical pulse-stimulation induced a transient increase in amperometric current (I_{amp}), followed by a subsequent decay to the baseline, representing transient DA release in the NAC (Fig. 2l). As expected, DA neuron-restricted KO of Syt11 in the VTA led to increased DA release in the NAC (Fig. 2l). To specifically assess DA vesicle recycling in the NAC, we employed an optogenetic approach by injecting FLEX^{loxP}-based Channelrhodopsin-2 (ChR2)-expressing AAV9 virus and TH-Cre virus

Fig. 2 | Syt11 deficiency at early ages mediates social deficits via dopamine over-transmission. **a** Schematic representation of virus injection (TH-Cre-EGFP, or TH-EGFP served as a control) into the VTA of neonatal Syt11-flox/flox mice (PO) for the generation of DA neuron-restricted Syt11-cKO mice from birth (Syt11 P0-cKO). **b** Representative micrograph showing the immunostaining of Syt11 (magenta) and TH (red) in a VTA-containing slice from a Syt11 P0-cKO mouse (6 weeks post virus injection) as described in **a**. Enlarged insets are shown on the right. $n = 3$ mice; Scale bars: 400 μm (left), 50 μm (right). **c** Representative Western blots and statistics showing the expression of Syt11 in the VTA of Syt11 P0-cKO mice compared to control mice. Scale bars, 400 μm . **d–f** Representative heat maps and statistics of the three-chamber social interaction test of juvenile (6–8 weeks) Syt11 P0-cKO *vs* control mice. **g–i** Representative heat maps and statistics of the social novelty test of juvenile Syt11 P0-cKO *vs* control mice. **j** Representative heat maps and statistics of sniffing time in the social approach test of juvenile Syt11 P0-cKO *vs* control mice. **k** Statistics of investigation frequency and investigation time in the home-cage social test of juvenile Syt11 P0-cKO *vs* control mice. **l** Schematic, representative amperometric currents (I_{amp}), and statistics showing DA release from DAergic terminals in the NAc of Syt11 P0-cKO ($n = 3$) *vs* control ($n = 3$) mice. Scale bars, 10 μm . **m** Left, schematic showing the co-injection of TH-Cre and DIO-ChR2-mCherry viruses into the VTA of juvenile (3 weeks) Syt11-flox/flox or wide-type mice to generate Syt11 3W-cKO ($n = 3$) or control ($n = 3$) mice with ChR2 expressed in VTA^{DA} neurons. Middle and right, representative paired-pulse stimulus (40 s)-evoked amperometric signals and statistics of the paired-pulse ratio showing the recycling of DA vesicles in NAc slices from Syt11 3W-cKO *vs* control mice. **n** Schematic

showing the co-injection of TH-Cre and DIO-hM3D-mCherry viruses into the VTA of juvenile (3 weeks) Syt11-flox/flox or wide-type mice to generate Syt11 3W-cKO ($n = 3$) or control ($n = 3$) mice with hM3D expressed in VTA^{DA} neurons. Middle and right, representative amperometric current (I_{amp}) traces and statistics of DA release in the mPFC of Syt11 3W-cKO *vs* control mice following CNO application (5 μM). **o** Schematic of virus injection (TH-Cre-EGFP or TH-EGFP) into the VTA of neonatal Syt11-flox/flox mice (PO) for the generation of Syt11 P0-cKO ($n = 8$) or control ($n = 4$) mice. Middle and right, representative AP traces and statistics of the spontaneous action potential firing rate of VTA DA neurons from Syt11 P0-cKO mice *vs* control mice. **p** Representative AP traces and statistics showing the excitatory effect of the D2R antagonist haloperidol (Halo, 50 nM) on DA neurons in VTA slices in situ from Syt11 P0-cKO ($n = 4$) *vs* control ($n = 4$) mice. **q** Representative AP traces and statistics showing the inhibitory effect of the D2R agonist quinpirole (Qp, 50 nM) on the excitability of DA neurons in VTA slices in situ from Syt11 P0-cKO ($n = 5$) *vs* control ($n = 5$) mice. **r** A working model showing that Syt11 deficiency increases DA transmission via \odot facilitating DA vesicle recycling, and \ominus decreasing surface auto-receptor D2R expression, which leads to increased excitability of DA neurons. Created in BioRender. Yang, C. (2023) <https://BioRender.com/w74v548>. Data are shown as box-and-whisker plots, with the median represented by the central line inside each box, the 25th and 75th percentiles represented by the edges of the box, and the whiskers extending to the most extreme data points. Ordinary two-way ANOVA followed by Bonferroni's multiple comparisons for (**e**, **h**) or two-tailed Mann-Whitney test for (**c**, **f**, **i–q**). * $P < 0.05$, ** $P < 0.01$, *** $P < 0.001$, n.s. no significant difference. Source data are provided as a Source Data file.

into the VTA of Syt11-floxed null or control mice. Notably, the paired-pulse ratio of DA release in NAc slices evoked by the 488-nm laser stimulus increased substantially in Syt11-cKO mice compared with control mice (Fig. 2m), validating accelerated vesicle recycling and hence elevated DA release in the NAc in the absence of Syt11.

We next assessed DA release in the mPFC by utilizing a clozapine-N-oxide (CNO)-based chemogenetic approach. TH-Cre and Cre-dependent hM3Dq-expressing AAV2/9 viruses were stereotaxically injected into the VTA of Syt11-floxed null or control mice (Fig. 2n). Immunostaining confirmed that the expression of mCherry/hM3Dq was restricted to DA neurons in the VTA (Supplementary information, Fig. S6a, b). Patch-clamp recordings revealed an elevated firing rate of DA neurons in the VTA upon CNO application (Supplementary information, Fig. S6c), while CFE recordings demonstrated that CNO application further elicited DA release in the mPFC (Fig. 2n). Similar with that in the NAc (Fig. 2l), the CNO-evoked DA release in the mPFC was higher in Syt11-cKO mice than in control mice (Fig. 2n). These results validate the elevated DA transmission and accelerated DA vesicle recycling upon Syt11 deficiency in DA neurons.

Moreover, electrophysiological patch-clamp recordings revealed a pronounced increase in the firing rate of action potentials (APs) of DA neurons in VTA slices from Syt11 P0-cKO mice (Fig. 2o), indicating the over-excitation of midbrain DA neurons in the absence of Syt11. Consistent with this, we also found the increased resting membrane potential (RMP) in VTA^{DA} neurons, with the membrane capacitance (Cm) and input membrane resistance (Rm) remained unchanged (Supplementary information, Fig. S7a). We hypothesized that the surface auto-inhibitory D2R receptor in DA neurons may undergo alterations due to the accelerated vesicle recycling^{27,28,30,34}. Consistent with our expectation, the facilitatory effect of the D2R antagonist haloperidol on AP firing of DA neurons was substantially diminished in VTA slices from Syt11 P0-cKO mice (Fig. 2p; Supplementary information, Fig. S7b). Similarly, we also observed a decreased inhibitory effect of the D2R agonist quinpirole on AP firing (Fig. 2q; Supplementary information, Fig. S7b), suggesting a reduction in functional D2R in DA neurons in situ in the absence of Syt11. In line with this, we also observed accelerated endocytosis with FM uptake (Supplementary information, Fig. S7c) and decreased expression of membrane D2R (Supplementary information, Fig. S7d, e) in Syt11 knockdown dopaminergic SY5Y cells, as well as the decreased total D2R expression in the VTA in Syt11-cKO mice (Supplementary information, Fig. S7f).

Although we couldn't fully exclude other possibilities (i.e. receptor signaling adaptations, gene expression alterations), our recent reports^{27,29,30} and the present findings collectively underscore that Syt11 deficiency leads to elevated DA transmission via accelerated endocytosis and vesicle recycling, as well as the hyperactivity of DA neurons due to the increased off-membrane trafficking of surface D2Rs (Fig. 2r).

DA neuron over-excitation during adolescence mediates schizophrenia-related social deficits

To further determine whether the over-excitation of VTA^{DA} neurons, which mimics elevated DA release, is sufficient to mediate schizophrenia-like social withdrawal, we performed co-injections of TH-Cre virus and Cre-dependent hM3Dq-expressing virus (with DIO-mCherry blank virus as a control) into the VTA of 3-week-old mice. These mice were then subjected to social behavior tests during adolescence (6–8 weeks) following the chemogenetic activation of DA neurons via intraperitoneal (i.p.) administration of CNO (Fig. 3a). Notably, a single dose of CNO was capable of significantly reducing the time spent sniffing the MI mouse in the three-chamber social test by hM3Dq-expressing mice (Fig. 3b, c). The social preference index was also decreased greatly compared to control virus-injected mice (Fig. 3d). Similarly, chemogenetic activation of VTA^{DA} neurons also resulted in inferior performance of hM3Dq-expressing mice in the social novelty test (Fig. 3e, f). Furthermore, the social interaction time with the stimulus mouse in the social approach test and with the stranger intruder mouse in the home-cage social test were both reduced in mice following chemogenetic activation (Fig. 3g, h), confirming that hyperactivity of DA neurons during early development is sufficient to cause social deficits. Importantly, mice with chemogenetic activation also exhibited aberrant PPI in the acoustic startle response and impaired short-term memory (Supplementary information, Fig. S8), further supporting the association between DA over-transmission and social withdrawal in schizophrenia. In contrast, similar chemogenetic activation of DA neurons failed to induce social deficits in adult mice in the three-chamber social interaction test (Supplementary information, Fig. S9a–c), social novelty test (Supplementary information, Fig. S9d, e), and home-cage social test (Supplementary information, Fig. S9f). These results demonstrate that transient over-excitation of VTA^{DA} neurons only mediates social withdrawal before late adolescence or young adulthood, suggesting a critical time window for DA

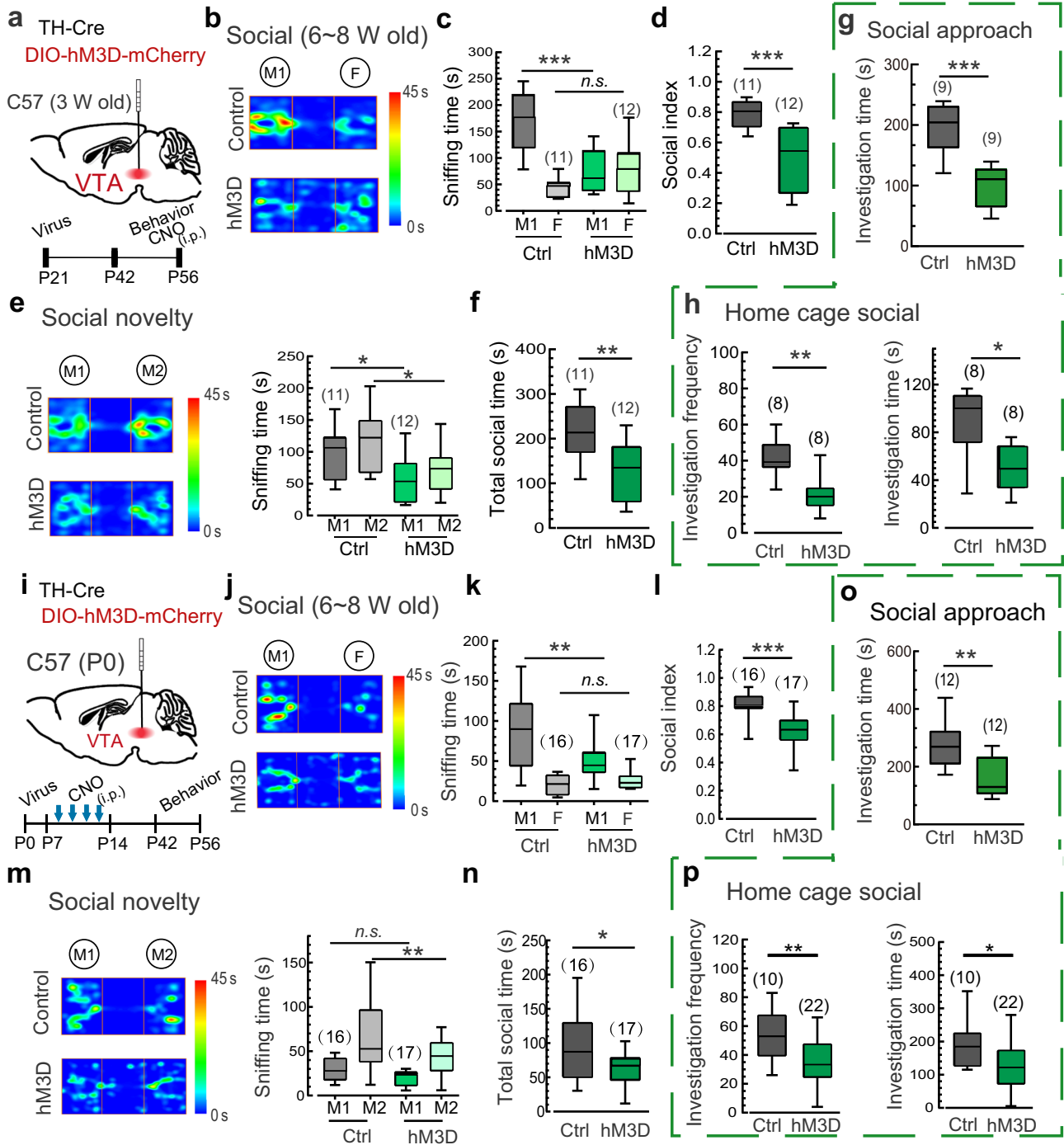


Fig. 3 | DA neuron over-excitation during adolescence mediates long-lasting social deficits. **a** Schematic showing the co-injection of TH-Cre and DIO-hM3D-mCherry/DIO-mCherry viruses into the VTA of juvenile (3 weeks) C57 mice. **b–d** Representative heat maps and statistics of the three-chamber social interaction test of juvenile (6–8 weeks) hM3D-expressing mice *vs* control mice following i.p. administration of CNO (0.5 mg/kg). **e**, **f** Representative heat maps and statistics of the social novelty test of juvenile hM3D-expressing mice *vs* control mice as described in **b–d**. **g** Statistics of sniffing time in the social approach test of juvenile hM3D-expressing mice *vs* control mice following i.p. administration of CNO. **h** Statistics of investigation frequency and investigation time in the home-cage social test of juvenile hM3D-expressing mice *vs* control mice following i.p. administration of CNO. **i** Schematic showing the co-injection of TH-Cre and DIO-hM3D-mCherry/DIO-mCherry viruses into the VTA of neonatal C57 mice (hM3D, P0) and the experimental procedure. **j–l** Representative heat maps and statistics of sniffing time and social index in the three-chamber social interaction test of juvenile

repetitive CNO-treated (every second day during P7–P14) hM3D-expressing mice *vs* control mice as described in **i**. **m**, **n** Representative heat maps and statistics of sniffing time and total social time in the social novelty test of juvenile repetitive CNO-treated hM3D-expressing mice *vs* control mice. **o** Sniffing time of juvenile repetitive CNO-treated hM3D-expressing mice *vs* control mice in the social approach test with a caged novel mouse. **p** Investigation frequency and investigation time of juvenile repetitive CNO-treated hM3D-expressing mice *vs* control mice in the home-cage social test. Data are shown as box-and-whisker plots, with the median represented by the central line inside each box, the 25th and 75th percentiles represented by the edges of the box, and the whiskers extending to the most extreme data points. Ordinary two-way ANOVA followed by Bonferroni’s multiple comparisons for (**c**, **e**, **k**, **m**), two-tailed Mann-Whitney test for (**d**, **f**, **h**, **l**, **n–p**). * $P < 0.05$, ** $P < 0.01$, *** $P < 0.001$, n.s. no significant difference. Source data are provided as a Source Data file.

hyperactivity in the pathogenesis of schizophrenia and implying a development-dependent shift of DAergic circuit/pathway in social behaviors.

We further explored whether over-excitation of DA neurons before early adolescence leads to long-lasting social deficits resembling those observed in individuals with schizophrenia. To this end, we performed co-injections of TH-Cre virus and Cre-dependent hM3Dq-expressing virus into the VTA during the early postnatal period (P0). Subsequently, systemic administration of CNO (i.p.) every second day from P7 to P14 was delivered to induce sustained over-excitation of DA neurons during the synapse maturation phase (Fig. 3i). Notably, compared with control mice, hM3Dq-expressing mice showed a significant reduction in the time spent sniffing the M1 mouse, consistent with the decreased social preference index in the three-chamber social test 4–6 weeks after the CNO treatment (Fig. 3j–l). Furthermore, these CNO-treated hM3Dq-expressing mice also displayed the reduced social preference for the stranger mouse (M2) and consequently the reduced total social time with both mice in the social novelty test (Fig. 3m, n). In line with these results, CNO-treated hM3Dq-expressing mice exhibited pronounced impairments in social interactions with the stimulus mouse in the social approach test and the stranger intruder mouse in the home-cage social test (Fig. 3o, p). These findings indicate that the social deficits induced by repetitive chemogenetic activation of VTA^{DA} neurons during the P7–P14 period can persist until at least young adulthood. Interestingly, the over-excitation of VTA^{DA} neurons was maintained at least 4 weeks following the repetitive chemogenetic activation (Supplementary information, Fig. S10), suggesting a long-lasting plastic change in the excitability of DA neurons. These findings suggest that environmental disturbances leading to DA over-transmission at an early age are sufficient to initiate persistent schizophrenia-like behaviors.

Schizophrenia has been reported to be more prevalent and severe in men than in women^{2,13}. Therefore, we investigated whether the over-excitation of DA neurons could similarly induce schizophrenia-like social withdrawal in female mice. Interestingly, repetitive chemogenetic activation of DA neurons before early adolescence resulted in persistent social deficits in female mice, ranging from late adolescence (Supplementary information, Fig. S11) to adulthood (Supplementary information, Fig. S12). These findings contradict the speculative ‘dual dysregulation’ of DA hypothesis¹⁵ and instead demonstrate that DA over-transmission is indeed a mechanism underlying social withdrawal. Considering the comprehensive schizophrenia-like behavioral changes observed in Syt11-cKO and Syt11 P0-cKO mice (Figs. 1 and 2; Supplementary information, Figs. S1–S5) and mice with DA neuron over-excitation (Figs. 2 and 3; Supplementary information, Figs. S6–S12), as well as the involvement of aberrant striatal DA release in the positive symptoms², these findings suggest a scenario in which DA over-transmission may represent a shared pathway contributing to different symptoms of schizophrenia during a critical time window before late adolescence.

DA over-transmission in the mPFC during adolescence mediates social deficits

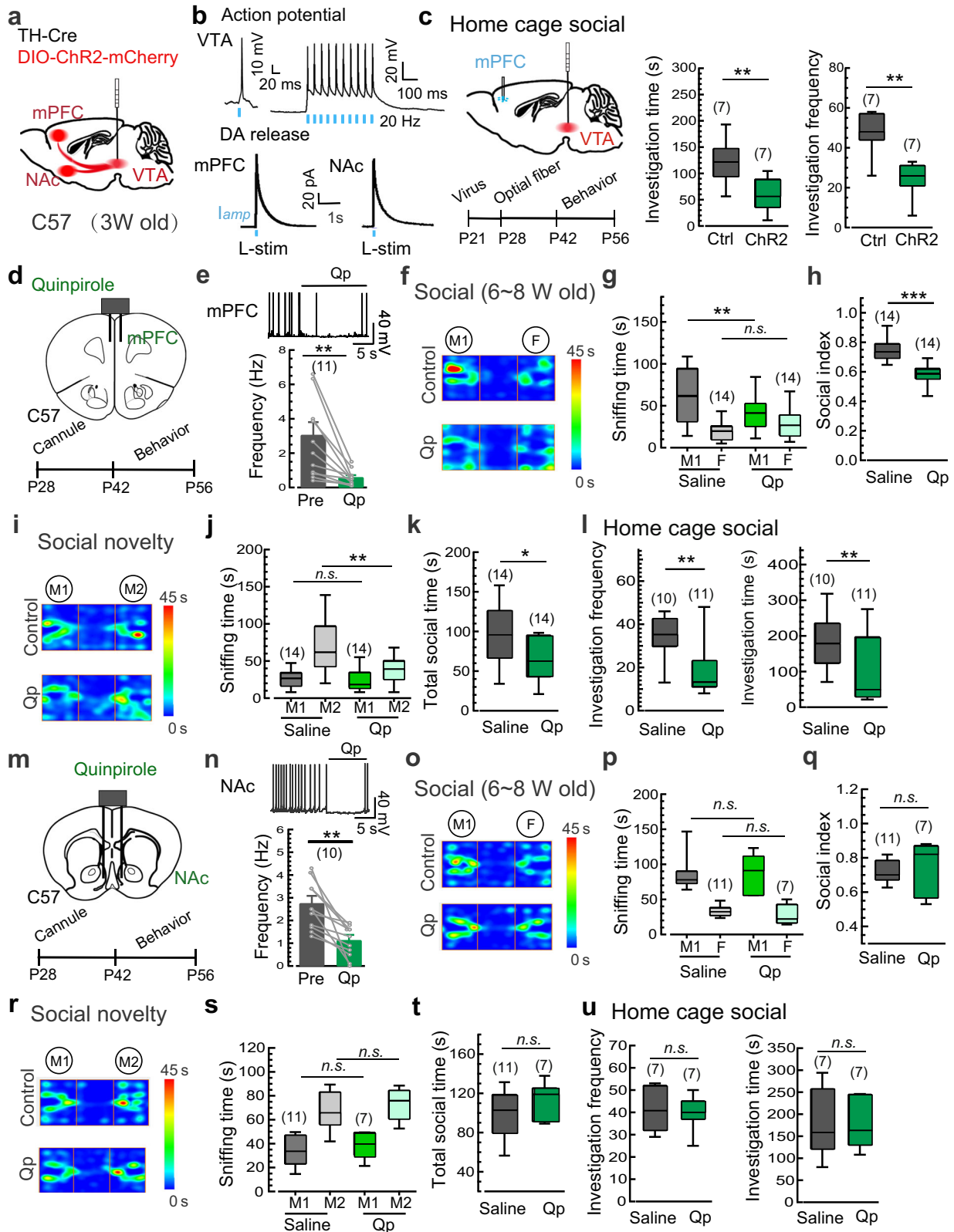
Given that the NAc and the mPFC are primary DA neuron-projecting regions involved in social behaviors, we used optogenetic manipulation to further determine the specific brain region downstream of VTA^{DA} neurons responsible for the social deficits in schizophrenia. The FLEX^{loxP}-based ChR2-expressing AAV9 virus and TH-Cre virus were co-injected into the VTA of 3-week-old mice (Fig. 4a). As expected, transient 473-nm light stimulation (L-stim, 1 ms duration) reliably elicited AP firing in DA neurons (mCherry-positive) in current-clamp electrophysiological recordings (Fig. 4b). Meanwhile, L-stim also triggered DA release in the NAc and mPFC, as detected by electrochemical amperometric recordings (Fig. 4b). Home-cage social test was carried out during the P42–P56 time window to evaluate the possible

contribution of the mPFC and NAc to the social deficits. Notably, a train of burst L-stim (5 ms, 8 pulses at 30 Hz; once every 5 s) on DA terminals in the mPFC resulted in a pronounced reduction in the social interaction with the intruder mouse (Fig. 4c). In contrast to the facilitatory effect of VTA-NAc DA signals on social behaviors in adult mice³⁵ (Supplementary information, Fig. S13), similar L-stim in the NAc failed to induce detectable changes in social interaction in adolescent mice (Supplementary information, Fig. S14), suggesting that the elevated DA release in the mPFC, but not the NAc, during adolescence mediates the social withdrawal downstream of VTA^{DA} neurons.

To further validate potential roles of DA over-transmission in the mPFC in social withdrawal, we assessed social deficits with pharmacological intervention targeting postsynaptic D2Rs in the mPFC (Fig. 4d). As expected³⁶, the local application of quinpirole, a potent D2R agonist, effectively reduced the activity of D2R-positive cortical neurons in mPFC slices (Fig. 4e). Subsequently, we conducted social behavior tests on adolescent mice following the stereotaxic injection of quinpirole (bilateral, 1 μg/μl, 0.2 μl per side) into the mPFC to augment DA transmission by activating postsynaptic D2Rs (Fig. 4d). As expected, quinpirole decreased the time spent in social interaction with the M1 mouse and the social preference index in the three-chamber social test (Fig. 4f–h). Similar inhibitory effects of quinpirole were observed in the social novelty test (Fig. 4i–k) and the home-cage social test (Fig. 4l). Conversely, the similar local infusion of quinpirole into the NAc (Fig. 4m, n) failed to induce impairments in social activities in the three-chamber social test (Fig. 4o–q), the social novelty test (Fig. 4r–t), and the home-cage social test (Fig. 4u). These findings confirm that DA over-transmission in the mPFC, but not the NAc, during adolescence plays a central role in mediating schizophrenia-like social deficits. The time window-specific inhibition of social preference by DA over-transmission in the mPFC suggests a role of DA transmission in the development and connectivity of mPFC neurons before late adolescence.

To validate potential roles of DA transmission in the plastic changes of mPFC neurons, we conducted assessments of morphological changes in the mPFC of Syt11 cKO mice. Consistent with the reduced cortical neurons and spine density observed in clinical studies^{37–39} and post-mortem evidence^{40–42}, we observed a significant decrease of MAP2-positive neurons in Layers I, II/III, and VI of the mPFC from Syt11 cKO mice (Fig. 5a, b). Accordingly, the intensity of TH-positive neurites in all Layers I–VI was substantially reduced (Fig. 5c, d). Consistent with this, although the density of VTA^{DA} neurons in Syt11 cKO mice remained unchanged (Supplementary information, Fig. S15a,b), the dendritic complexity of these neurons decreased greatly (Supplementary information, Fig. S15c,d). In line with these findings, repetitive chemogenetic activation of VTA^{DA} neurons during P7–P14 induced similar long-term changes in MAP2-positive neurons and TH-positive neurites in the mPFC (Supplementary information, Fig. S16a–d). These results suggest that DA over-transmission in the mPFC at early ages is sufficient to induce neurostructural alterations in the mPFC. Subsequently, we performed patch-clamp electrophysiological recordings to assess the functional changes of mPFC cortical neurons. Consistent with the reduced cortical excitability observed in schizophrenia⁴³, we indeed found the decreased excitatory postsynaptic current (Fig. 5e, f) and the decreased AP firing rate of mPFC cortical neurons in both adult Syt11 P0-cKO and CNO-treated (P7–P14) hM3Dq-expressing mice (Fig. 5g, h). These findings suggest that DA over-transmission before early adolescence leads to long-lasting morphological and functional plastic changes in mPFC cortical neurons.

To gain insights into mechanisms underlying the schizophrenia-like behavioral changes observed in Syt11 cKO mice, we performed genome-wide RNA-sequencing analysis to capture transcriptome-wide alterations in the mPFC of adult (3 months) Syt11 cKO mice. By comparing the gene expression profile of control (DAT-Cre) mice, we



identified 170 differentially expressed genes (DEGs) in Syt11-cKO mice (Fig. 5i, j). Among these DEGs, 97 were upregulated and 73 were downregulated. Interestingly, some of the detected DEGs, such as *Nrg1*, *Arc*, *Ddc* and *Icam*, are well-characterized schizophrenia risk genes that play critical roles in neural development and/or are functionally involved in the pathogenesis of schizophrenia^{44–47}. Gene ontology (GO) analysis revealed that DEGs were enriched in cellular components involved in

vesicle trafficking, such as the vesicle tethering complex, extracellular vesicles, and extracellular exosomes (Fig. 5k). In the biological process category, the enriched GO terms were strongly suggestive for processes related to vesicular trafficking (e.g. vesicle transport, axonal protein transport, post-synaptic retrograde transport, and vesicle-mediated intercellular transport), neurotransmission (e.g. DA biosynthetic process, membrane docking, synaptic transmission, synaptic

Fig. 4 | DA over-transmission in the mPFC during adolescence mediates schizophrenia-like social deficits. **a** Schematic of the co-injection of TH-Cre and DIO-ChR2-mCherry viruses into the VTA of juvenile C57 mice (3 weeks). **b** Upper, representative AP traces showing optogenetic activation of DA neurons in VTA slices (mCherry-positive) by 473-nm light stimulation (L-stim). Lower, representative amperometric traces showing the L-stim induced DA release in the NAc and mPFC slices. Data from 3 mice. **c** Schematic and statistics of sniffing time/frequency in the home-cage social test of the ChR2-expressing mice *vs* control mice following L-stim trains in the mPFC. **d** Schematic of bilateral cannula application of the D2R agonist quinpirole (Qp) into the mPFC and the experimental procedure. **e** Representative AP traces and statistics showing the inhibitory effect of Qp (50 nM) on the excitability of D2R-positive cortical neurons in the mPFC (Data from 3 mice and presented as mean \pm SEM). **f–h** Representative heat maps and statistics of the three-chamber social interaction test of juvenile (6–8 weeks) mice following the local application of Qp *vs* saline in the mPFC. **i–k** Representative heat maps and statistics of the social novelty test of the Qp- *vs* saline-treated juvenile mice as described in **f–h**. **l** Statistics of investigation frequency and investigation time in the

home cage social test of the Qp- *vs* saline-treated juvenile mice. **m** Schematic of bilateral cannula application of Qp into the NAc and the experimental procedure. **n** Representative AP traces and statistics showing the inhibitory effect of Qp (50 nM) on the excitability of D2R-positive cortical neurons in the NAc (Data from 3 mice and presented as mean \pm SEM). **o–q** Representative heat maps and statistics of the three-chamber social interaction test of juvenile (6–8 weeks) mice following the local application of Qp *vs* saline in the NAc. **r–t** Representative heat maps and statistics of the three-chamber social novelty test of juvenile mice following the local application of Qp *vs* saline in the NAc. **u** Investigation frequency and investigation time in the home cage social test of juvenile mice following the local application of Qp *vs* saline in the NAc. Data are shown as box-and-whisker plots, with the median represented by the central line inside each box, the 25th and 75th percentiles represented by the edges of the box, and the whiskers extending to the most extreme data points. Ordinary two-way ANOVA followed by Bonferroni's post-hoc test for (**g**, **j**, **p**, **s**), paired two-tailed Student's *t*-test for (**e**, **n**), or two-tailed Mann-Whitney test for (**c**, **h**, **k**, **l**, **q**, **t**, **u**), * $P < 0.05$, ** $P < 0.01$, *** $P < 0.001$, n.s. no significant difference. Source data are provided as a Source Data file.

plasticity, signal transduction, neurotransmitter receptor metabolic process, receptor signaling pathway, and post-synapse organization), and neural development (e.g. neural projection development, embryonic brain development, and nervous system development) (Fig. 5k). Consistently, repetitive chemogenetic activation of VTA^{DA} neurons during P7–P14 induced similar long-term transcriptome-wide changes in the mPFC (Supplementary information, Fig. S16e–g). Overall, the transcriptome sequencing analysis provides genetic insights into the long-term changes in the mPFC that are linked with Syt11 deficiency and/or DA over-transmission.

Pathogenic effects of the D2R antagonist haloperidol on social deficits

Haloperidol primarily alleviates positive symptoms by antagonizing D2 receptors and reducing elevated DA transmission in the striatum⁴⁸, but its efficacy is limited and is often accompanied by adverse effects, including the worsening of negative symptoms⁵. Given that D2Rs also act as inhibitory auto-receptors in DA neurons⁴⁹, we hypothesized that in addition to its therapeutic effect by antagonizing postsynaptic D2Rs, haloperidol may have an additional pathogenic effect on negative symptoms by removing the auto-inhibition of presynaptic/somatic D2Rs in DA neurons (Fig. 6a). Our patch-clamp recordings indeed showed that haloperidol application greatly increased the firing rate of DA neurons in the VTA (Supplementary information, Fig. S17). To further confirm the impact of haloperidol on DA release, we conducted electrochemical CFE recordings in the mPFC *in vivo* following electric stimulation of DA axons in the medial forebrain bundle. Notably, systemic administration of haloperidol (0.4 mg/kg) substantially enhanced evoked DA release in the mPFC (Fig. 6b), confirming the drug's ability to induce aberrant DA release *in vivo*. Thereby, the increased DA levels led to a decrease in the firing rate of cortical neurons in the mPFC (Fig. 6c), exhibiting an opposite effect on cortical neuron excitability compared to the direct antagonism of postsynaptic D2Rs. Consistent with these findings, local application of haloperidol onto mPFC slices resulted in both increased (55%, post-synaptic effect) and decreased (20%, pre-synaptic effect) excitation of cortical neurons (Fig. 6d), indicating a mixed effect of haloperidol in the mPFC with the postsynaptic effect being predominant.

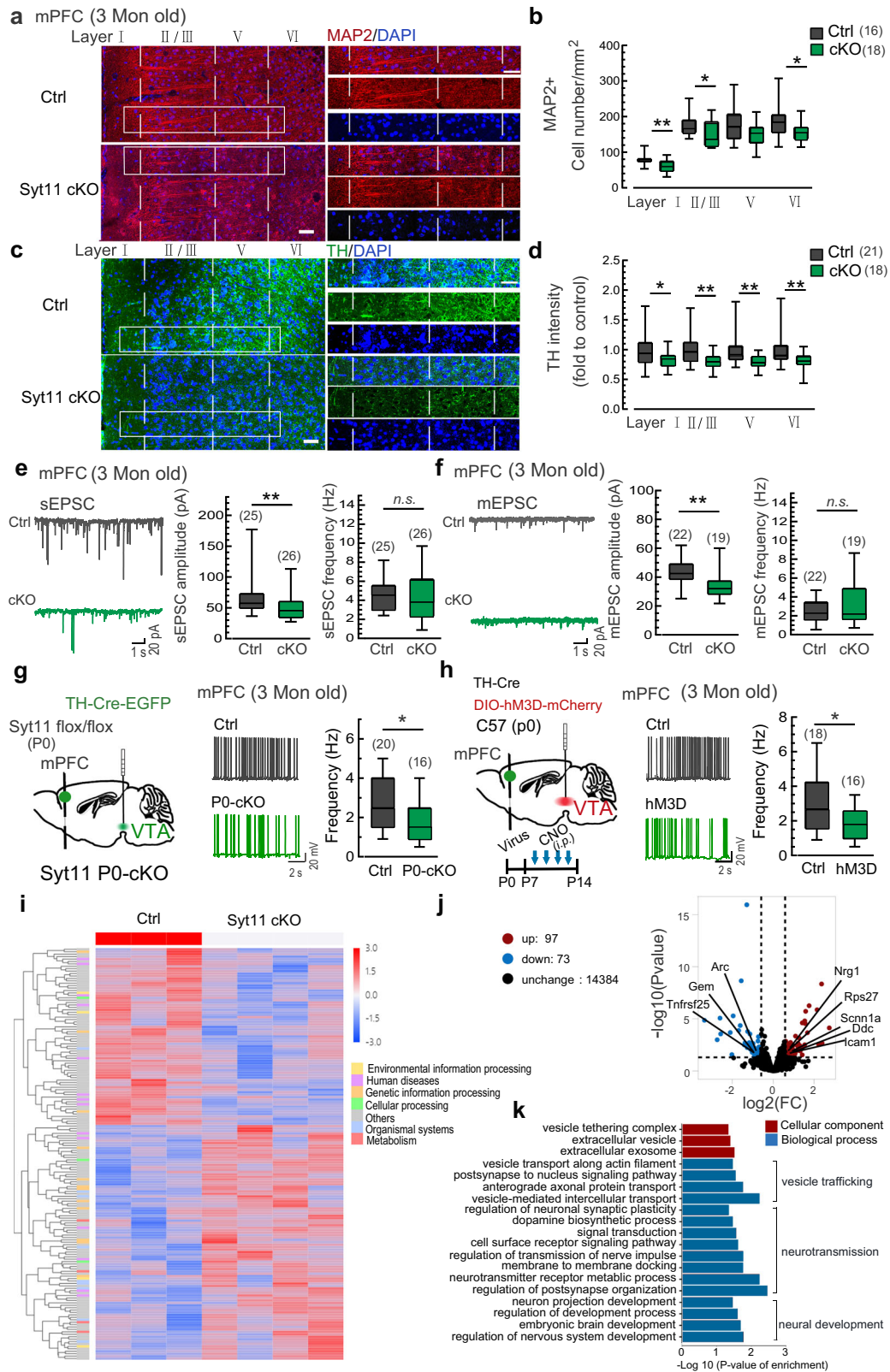
Regarding opposing roles of presynaptic and postsynaptic D2Rs in DA transmission, we postulated that the lack of efficacy of haloperidol and other antipsychotic agents in treating negative symptoms of schizophrenia could be attributed to their dual disinhibitory effects on both presynaptic/somatic and postsynaptic D2Rs. To investigate this, we tested whether the modulation of presynaptic/somatic D2Rs by locally delivering the clinical drug haloperidol into the VTA (thereby removing the auto-inhibition of DA neurons) could induce schizophrenia-like social withdrawal in adolescent mice (Fig. 6e).

Consistent with chemogenetic manipulations, pharmacological activation of DA neurons with a single local-delivery of haloperidol into the VTA (bilateral, 50 μ M) resulted in impaired social behaviors, including reduced social interaction time with the M1 mouse and a decreased social preference index in the three-chamber social test (Fig. 6f–h). Similarly, haloperidol infusion into the VTA also attenuated social preference for the stranger mouse (M2) and total sniffing time with both mice (Fig. 6i–k). Moreover, pretreatment with haloperidol in the VTA impaired social interaction with a stranger intruder mouse in the home-cage social test (Fig. 6l). Therefore, systemic treatment with haloperidol or other antipsychotic agents targeting D2Rs may inadvertently exacerbate schizophrenia-associated symptoms by promoting the over-excitation of DA neurons and thus the increased DA release. These results further support a role of DA over-transmission during adolescence in the pathogenesis of schizophrenia.

D2R as a dual therapeutic target for the treatment of schizophrenia

Considering the opposing roles of presynaptic and postsynaptic D2Rs in DA transmission, we propose that local administration of haloperidol or other D2R antagonists in the mPFC could be an effective approach to alleviate negative symptoms by rectifying the aberrant DA transmission postsynaptically (with a mixed effect, but the postsynaptic effect predominated as shown in Fig. 6d). To test this hypothesis, we locally infused haloperidol into the mPFC during the period of P42–P56 and monitored its impact on the social behaviors of Syt11 P0-cKO mice (Fig. 7a). Notably, a single administration of haloperidol into the mPFC restored the decreased social interaction with the M1 mouse and the reduced social preference index in Syt11 P0-cKO mice (Fig. 7b, c). Similarly, the diminished social preference for the stranger mouse (M2) and the total sniffing time with both mice were completely attenuated (Fig. 7d, e). Furthermore, compared with the impaired social interaction observed in saline-control Syt11 P0-cKO mice, the haloperidol-treated cKO mice exhibited a social interaction time indistinguishable from that of control mice in the home-cage social test (Fig. 7f). Therefore, local application of a D2R antagonist into the mPFC before late adolescence (or early adulthood) can rescue the schizophrenia-like social deficits. These findings not only provide a reasonable explanation for the limited effectiveness of well-known antipsychotics in alleviating negative symptoms in schizophrenia, but also propose a potential therapeutic strategy for the clinical treatment of the disease.

The present study has provided direct *in vivo* evidence that DA over-transmission during preadolescence is a risk factor in initiating the pathogenesis of schizophrenia (Figs. 1–4). Therefore, it is plausible to reverse the social deficits by locally delivering a D2R agonist into the VTA, which inhibits DA neurons by targeting somatic D2Rs, to rectify



the hyperactivity of DA neurons during this period. Similar to the effects of haloperidol in the mPFC, local delivery of the D2R agonist quinpirole into the VTA also demonstrated a therapeutic effect in adolescent Syt11 P0-cKO mice (Fig. 7g). Specifically, compared to the impaired social preference of Syt11 P0-cKO mice injected with saline, quinpirole-treated P0-cKO mice showed intact social interaction with the M1 mouse and an unchanged social preference index (Fig. 7h, i). In

addition, local application of quinpirole in the VTA fully reversed the pronounced social withdrawal of Syt11 P0-cKO mice in the social novelty test (Fig. 7j, k). Moreover, social interaction with the stranger intruder mouse in the home-cage social test was substantially attenuated by the local administration of quinpirole (Fig. 7l).

To further validate the therapeutic effect of quinpirole in the VTA, we utilized dizocilpine (MK-801)-induced schizophrenia-like mice.

Fig. 5 | Syt11 cKO and DA over-transmission lead to long-lasting structural and functional alterations in the mPFC. **a, b** Representative micrographs and statistics of MAP2-positive neurons in the mPFC of adult Syt11-cKO ($n = 6$) vs control ($n = 5$) mice. Scale bars: 50 μm for left, 20 μm for right. **c, d** Representative micrographs and statistics of TH-positive neurites in the mPFC of adult Syt11-cKO ($n = 6$) vs control ($n = 5$) mice. **e** Representative sEPSC traces and statistics of the amplitude and frequency of sEPSC in mPFC cortical neurons from adult Syt11-cKO ($n = 6$) vs control ($n = 6$) mice. **f** Representative mEPSC traces and statistics of the amplitude and frequency of mEPSC in mPFC cortical neurons of adult Syt11-cKO ($n = 6$) vs control ($n = 6$) mice. **g** Left, schematic of virus injection (TH-Cre-EGFP/TH-EGFP) into the VTA of neonatal Syt11-flox/flox mice (P0) for the generation of Syt11 P0-cKO or control mice. Middle and right, representative AP traces and statistics of spontaneous AP firing rates in mPFC cortical neurons of adult (3 months) Syt11 P0-cKO ($n = 4$) vs control ($n = 3$) mice. **h** Left, schematic showing the co-injection of TH-Cre and DIO-hM3Dq-mCherry/DIO-mCherry viruses into the VTA of neonatal C57

mice (hM3D, P0) and the experimental procedure. Middle and right, representative AP traces and statistics of spontaneous AP frequency in mPFC cortical neurons of adult repetitive CNO-treated hM3Dq-expressing ($n = 5$) vs control ($n = 4$) mice. **i** The heatmap showing gene expression profiling determined by genome-wide RNA sequencing (RNA-Seq) of the mPFC in Syt11 cKO ($n = 4$) vs control ($n = 3$) mice. Rows represent differentially expressed genes (DEGs), and columns represent transcriptomic profiles of individual animals. **j** Volcano plots showing gene expression profiling of the mPFC in Syt11 cKO vs control mice. The x-axis represents \log_2 fold change (FC) between the two groups. **k** Ingenuity gene ontology (GO) analysis indicating significantly enriched GO terms in cellular components and biological processes. Data are shown as box-and-whisker plots, with the median represented by the central line inside each box, the 25th and 75th percentiles represented by the edges of the box, and the whiskers extending to the most extreme data points. Two-tailed Mann-Whitney test, * $P < 0.05$, ** $P < 0.01$, *** $P < 0.001$, n.s. no significant difference. Source data are provided as a Source Data file.

Consistent with our hypothesis, pre-treatment with MK-801 indeed increased DA overflow in mPFC slices (Supplementary information, Fig. S18a, b), while MK-801 administration during preadolescence led to long-lasting social behavior deficits, which were fully reversed by the local application of quinpirole in the VTA (Supplementary information, Fig. S18c). Importantly, local application of quinpirole in the VTA to diminish the enhanced DA transmission to post-synaptic D2R neurons reversed sensory gating dysfunction in the MK801-induced schizophrenia mouse model (Supplementary information, Fig. S18d). These results further confirm the role of DA over-transmission before late adolescence in the development of schizophrenia and propose a therapeutic strategy targeting D2Rs for the clinical treatment of the disorders. Collectively, the present work suggests that both the pre-synaptic/somatic application of D2R agonists in the VTA and the postsynaptic delivery of D2R antagonists in the mPFC represent promising therapeutic approaches for the clinical treatment of schizophrenia-associated social withdrawal.

Long-lasting rescue of social withdrawal by targeting pre-synaptic or postsynaptic D2Rs

We have successfully demonstrated that the rectification of DA transmission via the brain region-specific intervention of D2Rs during adolescence can effectively reverse social deficits in schizophrenia. To investigate the long-lasting effects of this therapeutic approach, we conducted repeated local administration of haloperidol in the mPFC every second day from P42 to P49. Notably, we observed sustained rescue effects on social behaviors in Syt11 P0-cKO mice (Fig. 8a-h). Specifically, the adult haloperidol-treated P0-cKO mice showed normal sniffing time with a stranger M1 mouse and an unchanged social preference index in the three-chamber social test, similar to control mice (Fig. 8b-d). In addition, they exhibited intact social preference for the stranger M2 mouse and normal total social time with both mice in the social novelty test (Fig. 8e-g). Consistent with these results, the social interaction time with a stranger intruder mouse was effectively restored in adult haloperidol-treated P0-cKO mice in the social approach test (Fig. 8h). These findings confirm a complete and long-lasting recovery of social deficits through the suppression of elevated DA transmission *via* local application of a D2R antagonist in the mPFC.

Next, we determined whether local delivery of a D2R agonist into the VTA during adolescence could also produce long-lasting rescue effects on social deficits in Syt11 P0-cKO mice (Fig. 8i). Interestingly, similar to the haloperidol treatment in the mPFC, repeated local treatment with the D2R agonist quinpirole into the VTA restored the impaired social interaction with the stranger M1 mouse and the reduced social preference index in the three-chamber test in Syt11 P0-cKO mice (Fig. 8j-l). Furthermore, the social preference for the M2 mouse and the total social time with both mice were indistinguishable between adult quinpirole-treated Syt11 P0-cKO mice and control mice

(Fig. 8m-o). Finally, the social approach test confirmed that the therapeutic effects of quinpirole on social withdrawal in Syt11 P0-cKO mice were maintained into adulthood (Fig. 8p). Taken together, these findings provide valuable insights into long-lasting therapeutic strategies for schizophrenia by targeting D2Rs either presynaptically or postsynaptically before late adolescence, offering potential benefit for the permanent recovery of schizophrenia in clinical treatment.

Discussion

While there is ongoing debate, it has been reported that aberrant DA transmission is involved in the manifestation of positive symptoms in schizophrenia, which can be effectively alleviated by drugs antagonizing D2Rs in clinical treatments⁵⁰. Nonetheless, the role of DA transmission in schizophrenia and the underlying mechanisms of negative symptoms remain largely unclear, making it challenging to identify suitable therapeutic targets. In this study, we identify that *SYT11* deficiency is a potential risk factor causally linked to schizophrenia, demonstrate plasma Syt11 as a potential biomarker for the diagnosis of schizophrenia, and present the Syt11-cKO mouse as a valuable genetic animal model for schizophrenia study. Importantly, we further define periadolescent DA over-transmission as a neural mechanism initiating the pathogenesis of schizophrenia (Supplementary information, Fig. S19). The chemogenetic excitation of VTA^{DA} neurons before late adolescence induced both acute and long-lasting social deficits, establishing a direct link between DA dysregulation and schizophrenia-related symptoms. We also show that local manipulation to tune down DA transmission with clinical drugs, either a D2R agonist in the VTA or an antagonist in the mPFC, before late adolescence can produce sustained rescue effects on social deficits in Syt11 cKO mice. Thus, this study not only provides a reasonable explanation for the limited efficacy of well-known antipsychotics in restoring negative symptoms of schizophrenia, but also offers two potential D2R-targeting strategies for the clinical treatment of schizophrenia (Supplementary information, Fig. S19).

Although numerous schizophrenia risk genes have been identified, few have been shown to individually mediate the pathogenic pathway, pending the mechanisms of this disorder due to the lacking of an ideal genetic animal model⁵¹. *SYT11*, encoding a non- Ca^{2+} -binding Syt, is located on chromosome locus Iq22 and has been identified as a major susceptibility locus for both familial and sporadic schizophrenia based on genome-wide scanning and case-control studies^{23,24}. Our previous studies have demonstrated that Syt11 inhibits endocytosis, vesicle recycling, and DA release, and its accumulation plays a central role in parkin-associated Parkinson's disease^{27,29,30}. The current work, by combining evidences from human samples and clinical data, identifies Syt11 as a potential risk factor closely associated with schizophrenia (Fig. 1a-h). Furthermore, we define plasma Syt11 as a valuable biomarker for the clinical diagnosis of schizophrenia (Supplementary information, Fig. S1). In our study, we employed a DA neuron-restricted

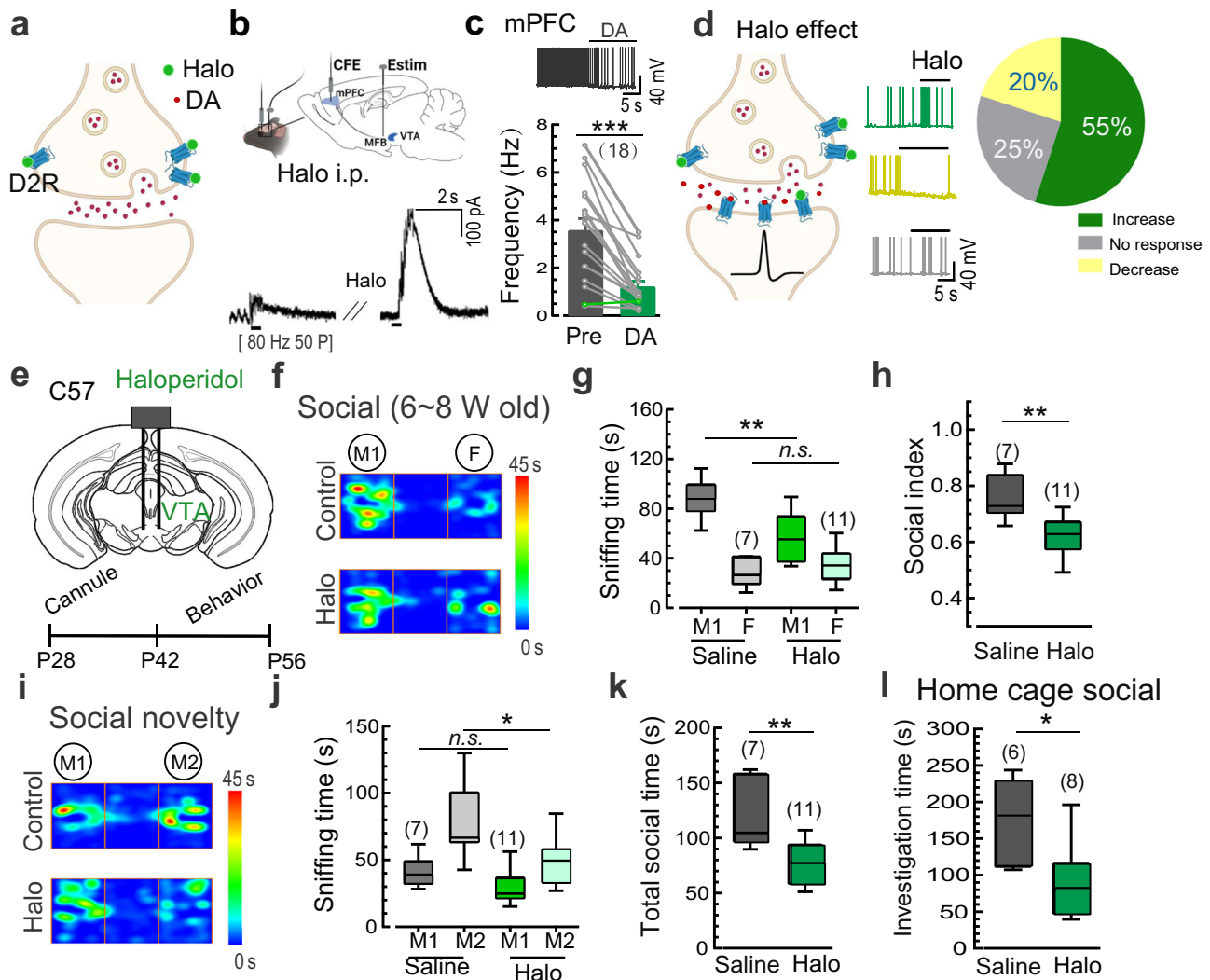


Fig. 6 | Pathogenic effects of the D2R antagonist haloperidol on social deficits.

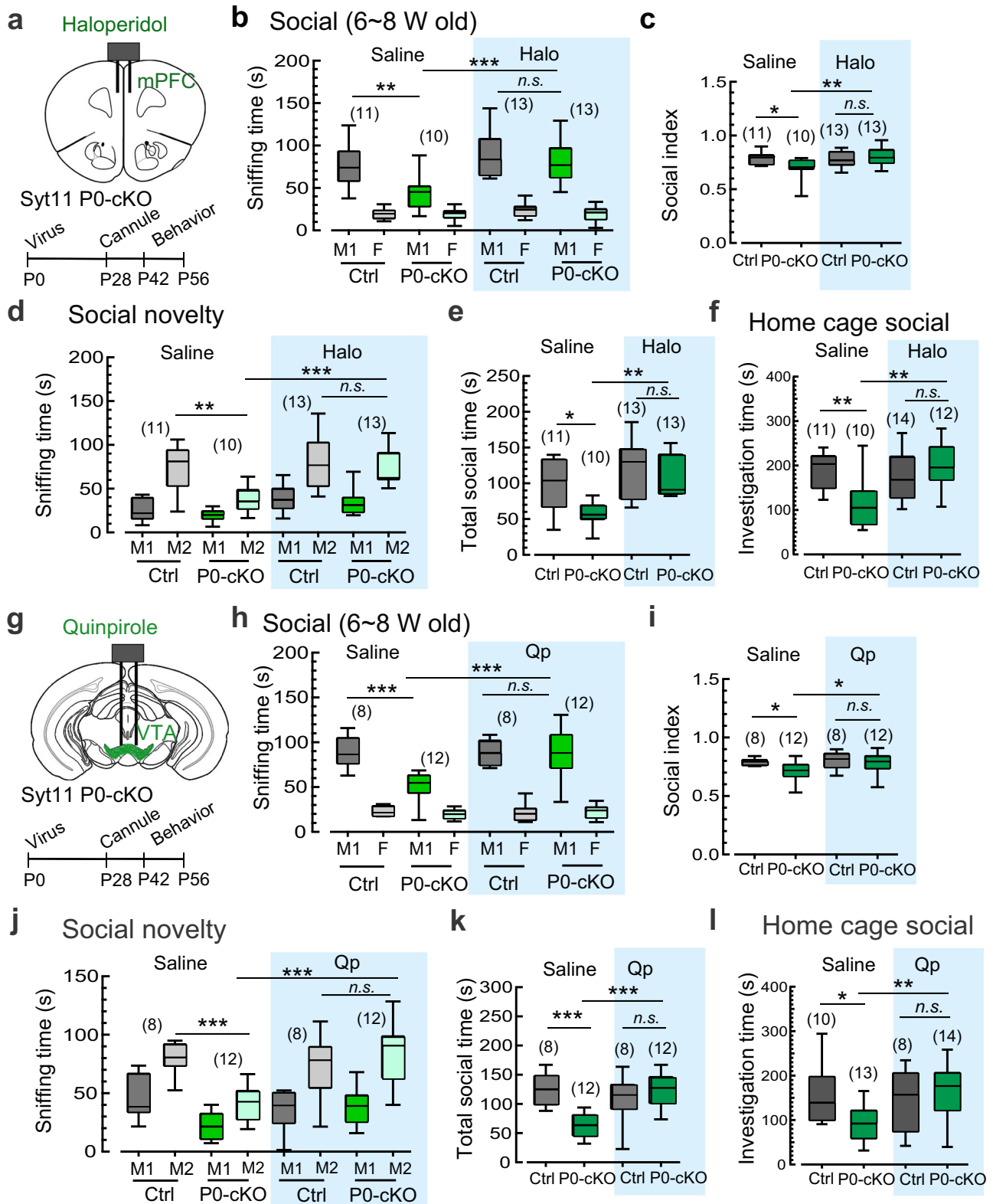
a Illustration showing the facilitatory effect of the D2R antagonist haloperidol (Halo) on DA transmission by targeting presynaptic D2Rs. **b** Schematic and representative traces showing increased DA release (evoked by a burst of electric stimulation [Estim, 50 pulses at 80 Hz] at the medial forebrain bundle) in the mPFC in vivo following i.p. application of Halo (0.4 mg/kg) in juvenile C57 mice. Data from 3 mice. **c** Representative trace and statistics of spontaneous APs of cortical neurons in mPFC slices in response to DA application (Data are presented as mean \pm SEM). Data from 4 mice. **d** Left, illustration showing the dual effects of Halo on DA transmission by targeting presynaptic and postsynaptic D2Rs. Middle and right, representative traces and statistics of spontaneous APs of mPFC cortical neurons in response to Halo application. Data from 3 mice. **e** Schematic of bilateral cannula application of Halo into the VTA and the experimental procedure. **f-h**

Representative heat maps and statistics of three-chamber social interaction time in juvenile (6–8 weeks) C57 mice following local application of Halo vs saline control in the VTA. **i-k** Representative heat maps and statistics of the social novelty test in Halo- vs saline-treated juvenile C57 mice. **l** Statistics of investigation time in juvenile C57 mice following local application of Halo vs saline control in the home-cage social test. Data are shown as box-and-whisker plots, with the median represented by the central line inside each box, the 25th and 75th percentiles represented by the edges of the box, and the whiskers extending to the most extreme data points. Ordinary two-way ANOVA followed by Bonferroni's post-hoc test for (**g**, **j**), two-tailed paired Student's *t*-test for (**c**), or two-tailed Mann-Whitney test for (**h**, **k**, **l**), **P* < 0.05, ***P* < 0.01, ****P* < 0.001, n.s. no significant difference. Source data are provided as a Source Data file.

knockout of *Syt11* and found that this alone is sufficient to mediate long-lasting social withdrawal (Fig. 1k-q; Supplementary information, Fig. S2a-j). This phenotype was accompanied with locomotion hyperactivity, sensorimotor gating disruption and cognitive decline without clear repetitive behaviors (Fig. 1r-u; Supplementary information, Fig. S2k-n), thus confirming roles of *Syt11* in the pathogenesis of schizophrenia. Although the locomotion hyperactivity may affect the performance in some of these behavioral tests, some of the key issues, such as sniffing/interaction time in multiple social tests and PPI are believed to be less dependent on locomotion activity^{52–54}. We also identified a critical time window for *Syt11* deficiency-mediated social deficits, occurring before late adolescence or young adulthood (Fig. 2a-k; Supplementary information, Figs. S3–S5), suggesting a potential role of *Syt11* in neural development, which aligns with the

well-documented brain developmental anomalies observed in schizophrenia. Therefore, our findings provide important insights into the pathogenesis of a subset of schizophrenia patients (~50%) with clear downregulation of *Syt11* and offer a mouse model for pre-clinical studies of schizophrenia.

Both our previous studies³⁰ and the present work have shown that *Syt11* deficiency leads to an elevated firing rate of DA neurons (via decreasing surface functional D2Rs) and enhanced DA release (via accelerating vesicle recycling) in the striatum, NAc and mPFC (Fig. 2l-r). Moreover, we found that over-excitation of VTA^{DA} neurons through chemogenetic (Fig. 3), optogenetic (Fig. 4a-c), or pharmacological (Figs. 4d-l; 6e-l) approaches is sufficient to mediate similar impairments in social behaviors. These results indicate that *Syt11* deficiency impairs social behaviors and other schizophrenia-related



symptoms, most probably via enhanced DA transmission. These results are at odds with a prior report that forebrain-specific Syt11-cKO mice only showed the impaired synaptic plasticity with no significant alteration in fast neurotransmitter release⁵⁵. Considering that we have validated pivotal roles of Syt11 in endocytosis and neural secretion in a variety of types of cells, ranging from primary sensory neurons, hippocampal neurons, midbrain DA neurons, to glia cells^{27,30,56}, the lack of a clear impairment in synaptic

transmission is probably attributed to the relatively lower level of Syt11 expression in forebrain cortical neurons⁵⁷. Considering the general role of Syt11 in endocytosis and neurotransmission and its ubiquitous expression in the brain^{27,30,56}, Syt11 expression in other cell types may also contribute to the pathogenesis of schizophrenia. Nonetheless, we have defined the enhanced DA transmission as a mechanism mediating Syt11 deficiency-induced pathogenesis of schizophrenia.

Fig. 7 | D2R serves as a dual therapeutic target presynaptically and postsynaptically for reversing schizophrenia-related social deficits. **a** Schematic of bilateral cannula application of the D2R antagonist haloperidol (Halo, 50 μ M) into the mPFC of juvenile Syt11 P0-cKO or control mice (TH-Cre-EGFP or TH-EGFP AAV injected into the VTA of neonatal Syt11 flox/flox mice) and the experimental procedure. **b, c** Statistics of the three-chamber social interaction test in Syt11 P0-cKO and control mice following local application of Halo *vs* saline in the mPFC. **d, e** Statistics of the social novelty test in Halo- *vs* saline-treated Syt11 P0-cKO and control mice. **f** Statistics of investigation time in Halo- *vs* saline-treated Syt11 P0-cKO and control mice in the home-cage social test. **g** Schematic of bilateral cannula application of the D2R agonist quinpirole (Qp, 1 μ g/ μ l) into the VTA of juvenile Syt11

P0-cKO and control mice and the experimental procedure. **h, i** Statistics of the three-chamber social interaction test in Syt11 P0-cKO and control mice following local application of Qp *vs* saline in the VTA. **j, k** Statistics of the social novelty test in Qp- *vs* saline-treated Syt11 P0-cKO and control mice. **l** Statistics of investigation time in Qp- *vs* saline-treated Syt11 P0-cKO and control mice in the home-cage social test. Data are shown as box-and-whisker plots, with the median represented by the central line inside each box, the 25th and 75th percentiles represented by the edges of the box, and the whiskers extending to the most extreme data points. Ordinary two-way ANOVA followed by Bonferroni's post-hoc test, * $P < 0.05$, ** $P < 0.01$, *** $P < 0.001$, n.s. no significant difference. Source data are provided as a Source Data file.

Although excess striatal DA release has long been proposed to be associated with positive symptoms of schizophrenia^{9,13,58–60}, the hyperfunction of the DA pathway has faced significant challenges and is proposed downstream of hyperactive glutamatergic projections or that of the excitatory-inhibitory imbalance of synaptic inputs^{8,11,60–62}. Importantly, pathophysiological mechanisms underlying negative and cognitive symptoms, particularly that of social withdrawal, remain unclear. As an alternative, the 'dual dysregulation' of DA alteration has been proposed as a reformulation of the DA hypothesis, in which the hypofunction of DA transmission in the prefrontal cortex has been implicated in negative and cognitive symptoms^{15,16,19,63}. However, this DA pathway has not been thoroughly assessed yet. The present work provides direct evidence that the over-excitation of DA neurons and the enhanced DA release in Syt11 cKO (Fig. 2) and MK801-induced (Supplementary information, Fig. S18a,b) schizophrenia mouse models are paralleled by schizophrenia-like social deficits. Additionally, chemogenetic activation of VTA^{DA} neurons before late adolescence is sufficient to mediate schizophrenia-like social deficits in both male (Fig. 3a–h) and female mice (Supplementary information, Figs. S11 and S12). Interestingly, repeated activation of VTA^{DA} neurons before early adolescence leads to long-lasting impairments in social behaviors up to late adolescence and adulthood (Fig. 3i–p; Supplementary information, Figs. S10–S12). These findings suggest that DA over-transmission plays an essential role in the pathogenesis of schizophrenia. Notably, over-excitation of DA neurons in adult mice fails to induce schizophrenia-associated social withdrawal (Supplementary information, Fig. S9), highlighting the importance of a critical time window for DA over-excitation in mediating the pathogenesis of the disorder. Furthermore, local pharmacological manipulation of DA transmission that reconciles with the enhanced DA release before late adolescence fully mitigates social disability in Syt11 P0-cKO mice (Fig. 7). This challenges the speculative 'dual dysregulation' of DA hypothesis¹⁵ and provides direct evidence that DA over-transmission is a mechanism initiating social withdrawal and other negative symptom-like behavioral changes. Taken together with the overall schizophrenia-like behavioral changes in Syt11-cKO and Syt11 P0-cKO mice (Figs. 1 and 2; Supplementary information, Fig. S2) as well as the involvement of aberrant striatal DA release in positive symptoms^{2,15}, these findings suggest that DA over-transmission may represent a common pathway for different symptoms of schizophrenia, particularly during a critical time window before late adolescence.

The NAc and the mPFC are primary DA neuron-projecting brain regions involved in social behavior. The activity of DA neurons projecting from the VTA to the NAc has been shown to be motivationally relevant with social stimuli and enhance social interaction in adult mice, probably through the reward circuit^{35,64}. However, whether DA release in the NAc also contributes to the social deficits in schizophrenia remain unclear. Although VTA^{DA}-NAc transmission facilitates social behaviors in adult mice (Supplementary information, Fig. S13), neither optogenetic activation of DA release (Supplementary information, Fig. S14) nor postsynaptic activation of D2Rs in the NAc (Fig. 4m–u) is capable of mediating social changes before adulthood. Instead, we found that either chemogenetic/pharmacological over-

excitation of VTA^{DA} neurons (Figs. 3 and 6e–l) or postsynaptic enhancement of DA transmission with the D2R agonist quinpirole in the mPFC (Fig. 4d–l) before late adolescence is sufficient to mediate social deficits. Importantly, optogenetic activation of DA release in the mPFC leads to similar social withdrawal in adolescent mice (Fig. 4a–c), while local application of the D2R antagonist haloperidol in the mPFC during adolescence completely and probably permanently rescues social deficits in Syt11 P0-cKO mice (Figs. 7a–f and 8a–h). Consistent with this, both Syt11-cKO and chemogenetic activation-mediated DA over-transmission before early adolescence led to similar long-lasting morphological, functional, and transcriptional plastic changes in the mPFC (Fig. 5; Supplementary information, Fig. S16), supporting an essential role of VTA-mPFC DA transmission in the pathogenesis of schizophrenia. Collectively, we have identified a time window-specific inhibition of social preference by DA over-transmission in the mPFC before late adolescence. Considering that local circuit in the mPFC is very complex^{65–71}, which specific type of D2R neurons and how they can mediate social impairments remain open questions. Excitation of DA neurons in the substantia nigra pars compacta (SNpc) has also been reported to cause deficits in social interaction⁷², implying that different DA circuits may be involved in the SCZ-onset mechanism. Nonetheless, the development-dependent switch from inhibitory (via the mPFC) to facilitatory (via the NAc) effects of DA transmission on social preference deserves systematic investigation in future.

Although antipsychotic reagents targeting D2Rs are effective for treating positive symptoms of schizophrenia⁷³, they have limited efficacy for negative and cognitive symptoms^{2,74}. This may be due to the fact that D2R antagonists can affect behavior either by dampening DA transmission in postsynaptic neurons in the mPFC or by enhancing the activity of VTA^{DA} neurons *via* inhibitory auto-receptors. Although haloperidol has been reported to block D2 auto-receptors for decades and is part of the established model of antipsychotic actions^{75,76}, whether and how pre-synaptic D2R auto-receptor contributes to the pathogenesis of and therapeutic effects on schizophrenia remain largely unknown. In the present work, we found that when the D2R antagonist haloperidol is delivered directly into the VTA during adolescence, it leads to the development of schizophrenia-like social deficits but fails to rectify them (Fig. 6; Supplementary information, Fig. S17). Alternatively, targeting DA transmission specifically in the mPFC, where the postsynaptic effect is dominant, may be a more effective approach to prevent social disorders in a broader manner. Importantly, we have found both the acute (Fig. 7a–f) and long-lasting (Fig. 8a–h) restoration of social withdrawal in Syt11 P0-cKO mice by locally delivering haloperidol into the mPFC during late adolescence. These findings offer a scenario explanation as to why traditional antipsychotic agents have not been successful in treating negative symptoms of schizophrenia and propose a potential therapeutic strategy for achieving complete and long-term recovery from the disease.

Based on our findings that DA over-transmission before late adolescence initiates the pathogenesis of schizophrenia (Figs. 1–6), it is plausible to alleviate social deficits by delivering a D2R agonist locally to the VTA to rectify the excitation of DA neurons during this critical period. Consistent with the hypothesis, we found that a single local

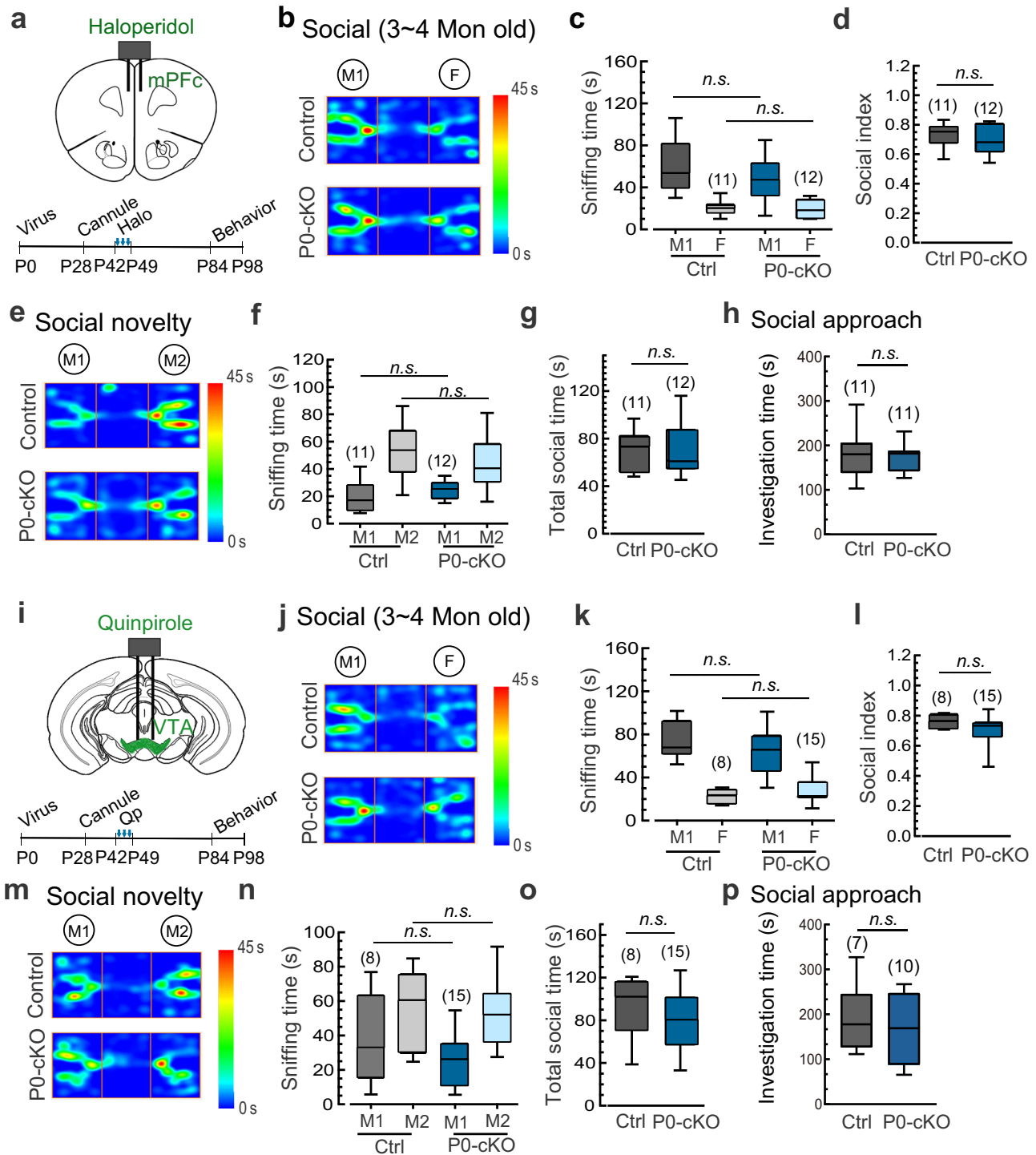


Fig. 8 | D2R serves as a dual therapeutic target exhibiting long-lasting rescue of social deficits. **a** Schematic of repetitive bilateral cannula application of a D2R antagonist (Halo) in the mPFC (every second day during P42-P49) and the experimental procedure for assessing social behaviors in Syt11 P0-cKO *vs* control mice. **b–d** Representative heat maps and statistics of three-chamber social interaction in adult (3–4 months) Halo-treated Syt11 P0-cKO *vs* control mice as described in **a**. **e–g** Representative heat maps and statistics of the three-chamber social novelty test in adult Halo-treated Syt11 P0-cKO *vs* control mice. **h** Statistics of investigation time of adult Halo-treated Syt11 P0-cKO *vs* control mice in the social approach test. **i** Schematic of repetitive bilateral cannula application of a D2R agonist (Qp) in the mPFC (every second day during P42-P49) and the experimental procedure for assessing social behaviors in Syt11 P0-cKO *vs* control mice. **j–l** Representative heat

maps and statistics of three-chamber social interaction test of adult (3–4 months) Qp-treated Syt11 P0-cKO *vs* control mice as described in **i**. **m–o** Representative heat maps and statistics of the three-chamber social novelty test of adult Qp-treated Syt11 P0-cKO *vs* control mice. **p** Statistics of investigation time of adult Qp-treated Syt11 P0-cKO *vs* control mice in the social approach test. Data are shown as box-and-whisker plots, with the median represented by the central line inside each box, the 25th and 75th percentiles represented by the edges of the box, and the whiskers extending to the most extreme data points. Ordinary two-way ANOVA followed by Bonferroni’s post-hoc test (**c, f, k, n**) or two-tailed Mann-Whitney test (**d, g, h, l, o, p**), * $P < 0.05$, ** $P < 0.01$, *** $P < 0.001$, n.s. no significant difference. Source data are provided as a Source Data file.

delivery of the D2R agonist quinpirole to the VTA during adolescence led to complete recovery from both social deficits and the impaired PPI in both Syt11 P0-cKO (Fig. 7g-l) and MK801-induced (Supplementary information, Fig. S18) schizophrenia mouse models. Importantly, repeated delivery of quinpirole specifically into the VTA during late adolescence also results in long-lasting restoration of social withdrawal (Fig. 8i-p). These findings confirm an essential role of DA transmission before late adolescence in the development of schizophrenia and suggest a potential D2R-targeting therapeutic strategy for the clinical treatment of the disorder. Given that aberrant striatal DA release underlies positive symptoms of schizophrenia, these findings not only indicate a common role of DA transmission in positive symptoms, negative symptoms, and cognitive aspects of schizophrenia but also open possibilities for clinical treatment of schizophrenia by targeting presynaptic DA release with D2R agonists.

In summary, we have identified Syt11 as a potential risk factor for schizophrenia, developed a mouse model for systematic schizophrenia study, and presented direct evidence demonstrating that DA over-transmission during a sensitive time window before late adolescence plays a pivotal role in initiating the pathogenesis of schizophrenia (Supplementary information, Fig. S19). These findings not only provide important inputs in understanding the onset and progression of social withdrawal but also contribute to the mechanisms underlying other negative symptoms and cognitive dysfunction, highlighting DA over-transmission as a common upstream trigger for neurodevelopmental anomalies in schizophrenia. Importantly, this study not only offers a reasonable explanation for the limited effectiveness of traditional antipsychotics in alleviating negative symptoms but also suggests two D2R-targeting strategies as potential treatments for schizophrenia.

Methods

Study approval

For human studies, prior to their participation, all subjects provided written informed consent. Our study was conducted in accordance with the ethical principles outlined in the 2002 Declaration of Helsinki and was approved by the Medical Ethics Committees of Xi'an Jiaotong University (NO. 2014-003). For all animal studies, the use and care of animals were conducted in accordance with the guidelines and regulations approved by the Animal Care and Use Committee of Xi'an Jiaotong University (NO.2016-10).

Subjects

To investigate Syt11 expression changes in schizophrenia, we obtained RNA-sequencing data from three datasets: LIBD dataset (175 schizophrenia patients and 318 healthy controls), CMC dataset (264 schizophrenia patients and 294 healthy controls), and HBCC dataset (97 schizophrenia patients and 220 healthy controls), as previously described by Hoffman et al³¹.

To validate the Syt11 expression changes observed in the RNA-sequencing data, we conducted qPCR and Western blot analyses using two independent sporadic case-control samples. The qPCR samples comprised 23 schizophrenia patients (12 females and 11 males) from the Xi'an Mental Health Center and 40 healthy controls (20 females and 20 males) from the Health Examination Center of the Second Affiliated Hospital of Xi'an Jiaotong University. To ensure the integrity of RNA for subsequent experiments, peripheral blood was collected using PAXgene tubes (BD Biosciences, USA) to prevent RNA degradation. The Western blot samples consisted of 30 schizophrenia patients (all males) and 30 age-matched healthy controls (all males) from the Psychiatric Unit and Health Examination Center of the First Affiliated Hospital of Xi'an Jiaotong University. Peripheral blood was collected using EDTA-containing tubes to prevent coagulation. All schizophrenia patients underwent standard diagnostic procedures and were confirmed by at least two experienced psychiatrists using the Structured

Clinical Interview for DSM-IV Axis I Disorders (SCID) and the Diagnostic and Statistical Manual of Mental Disorders, Fifth Edition (DSM-V). Patients were excluded from the study if they exhibited substance abuse, suicidal tendencies, abnormal laboratory results or ECG/EEG readings, or had a significant medical history such as brain surgery, unstable somatic conditions, or viral infections. Patients who had taken antipsychotic medication within one month prior to the recruitment were also excluded. Healthy controls were individually interviewed using the Structured Clinical Interview for DSM-IV-TR Axis I Disorders Non-Patient Edition (SCID-NP) to ensure the absence of any mental disorders. They self-reported no physical illness or personal/family history of psychiatric disorders.

In accordance with the aforementioned diagnostic and exclusive criteria, we recruited inpatients diagnosed with schizophrenia from the Yulin Mental Health Center to form our third independent sample. These inpatients had been receiving conventional antipsychotic treatment (Haloperidol, Olanzapine, or Risperidone) for a minimum of eight weeks, and treatment efficacy was assessed using the Positive and Negative Syndrome Scale (PANSS), as documented in their medical records. The choice of anti-schizophrenia medication was determined by the attending physician based on the individual patient's condition. In our study, we collected peripheral blood samples from each patient using PAXgene tubes (BD Biosciences, USA) at two time points (before and after treatment). It is important to note that haloperidol is no longer considered a first-line treatment option for schizophrenia in China. It is now reserved for cases where patients exhibit severe positive symptoms and initially show uncooperative with the treatment. For clarity, those patients who received a combination of haloperidol and olanzapine in our study are referred to as the 'haloperidol group'. Finally, a total of 20 schizophrenia inpatients (10 females and 10 males) were included and were assigned to one of the three treatment groups (haloperidol, olanzapine, or risperidone) based on individualized treatment plans prescribed by their attending physicians, taking into consideration their respective symptom conditions.

Animals

The floxed Syt11-null mice used in this study were obtained from The Jackson Laboratory (strain B6.129-Syt11tm1Sud/J). DAT-Cre transgenic mice (strain B6.SJL-Slc6a3tm1.1(cre) Bkmn/J) were kindly provided by Dr. Minmin Luo (National Institute of Biological Science, China)⁷⁷. Male or female C57BL/6J (B6) mice were sourced from Charles River Laboratories. Heterozygous DAT-Cre mice were used as control of Syt11 cKO mice. Control viral infection in floxed Syt11-null mice was used as a control of Syt11 P0-cKO or Syt11 adult-cKO mice. Both male and female mice were used as indicated in the study. All mice were housed in the animal facility, maintained under a 12-h light/dark cycle at 22 ± 2 °C and 40–60% humidity, and provided with ad libitum access to food and water. The mice were finally euthanized with CO₂, followed by cervical dislocation.

Cell culture and transfection

Human neuroblastoma SH-SY5Y cells (ATCC® CRL-2266™) were originally sourced from the ATCC. They were cultured in Dulbecco's modified Eagle's medium-F12 supplemented with 10% fetal bovine serum at 37 °C with 5% CO₂. For Syt11 knockdown, Syt11-shRNA carrying or scrambled control AAV virus (Shanghai OBiO Technology Corp., Ltd.) were used to infect SH-SY5Y cells when cells reached ~75% confluence. Immunoblotting was performed 3 days after transfection.

FM uptake

FM1-43 uptake was performed as described previously²⁷. Cells were washed 3 times with standard extracellular bath solution and then incubated with 10 μM FM1-43 in standard or high K⁺ (100 mM) -containing external solution at room temperature. Then washed out with

the standard bath solution after incubation. The external solution contained (in mM) 150 NaCl, 5 KCl, 2.5 CaCl₂, 1 MgCl₂, 10 H-HEPES, and 10 D-glucose, pH 7.4. In 100 mM K⁺ external solutions, the NaCl concentration was reduced to maintain the same ionic strength. Fluorescence images were captured on a Leica TCS SP8 STED inverted confocal microscope (Leica, Germany). The FMI-43 fluorescence intensity was calculated with the software of Image J.

Stereotaxic cannulation surgery

Male adolescent mice (3–4 weeks old for cannula implantation and 5–6 weeks old for optical fiber implantation) were anesthetized with avertin (10 mg/kg, i.p.). To maintain their body temperature at a constant 37 °C, a heating pad (KEL-2000, Nanjing, China) was used. The mice were then carefully secured in a stereotaxic apparatus (Narishige Inc., Japan), and the head position was adjusted to realize the same height of the skull surfaces of Bregma and Lambda. Craniotomies were meticulously performed using a cranial drill (RWD Instruments, China) for the implantation of guide cannulas or optical fibers. The cannulas were bilaterally implanted over the NAc (in mm: AP +1.25, ML +/−0.75, DV −4.3), the mPFC (in mm: AP +2.8, ML +/−0.5, DV −1.7), or the VTA (in mm: AP −3.4, ML +/−0.5, DV −4.4). In juvenile or adolescent mice, these coordinates were correspondingly adjusted based on the proportional relation between the measured distance from the bregma and lambda and its default value (4.2 mm) in adult mice. For optical stimulation of VTA projections in the NAc or mPFC, an optical fiber was carefully implanted into the lateral NAc and the prelimbic region of the mPFC.

Stereotactic virus injection

Both adolescent (3–4 weeks old) and adult (3–4 months old) male mice were anesthetized with avertin (10 mg/kg, i.p.), and their body temperature was carefully maintained at a constant 37 °C using a heating pad (KEL-2000, Nanjing, China). Then, they were securely placed in a stereotaxic apparatus equipped with a mouse adapter (Narishige Inc., Japan), and the head position was adjusted to realize the same height of the skull surfaces of Bregma and Lambda. Meticulous craniotomies were performed using a cranial drill (RWD Instruments, China) to minimize any potential damage to the cortical tissue. The virus (2–5 × 10¹² vg/ml, 500 nl) was stereotaxically injected into the middle region of the VTA (AP: −3.2 mm, ML: 0 mm, DV: −4.5 mm) according to the coordinates described above with a glass micropipette. The injection site in juvenile mice was adjusted nearby (AP −2.8 mm, ML 0 mm, DV −3.7 mm) according to the distance between bregma and lambda. The infusion rate (100 nl/min) was precisely controlled using a nanoliter injection pump (RWD, China). The micropipette was kept stationary for 15 min before slow withdrawal. The micropipettes were fabricated by glass capillary tubes (Narishige Inc., Japan) with a tip diameter of ~20 μm. For postnatal day 0–1 (P0, male or female as indicated) mice, the overall procedure of stereotaxic injections was the same with some modifications. The pup mice were anesthetized by deep hypothermia with ice and securely positioned in a stereotaxic frame (Narishige, Japan) with a pair of soft faceplates. The dosage of virus is 150 nl (2–5 × 10¹² vg/ml) for each pup mouse. The coordinate of VTA for injection was adjusted correspondingly (0.1 mm anterior, and 3.7 mm ventral to lambda).

Acute slice preparation

The mice were anesthetized with avertin (10 mg/kg, i.p.) and transcardially perfused with ~5 ml ice-cold cutting artificial cerebrospinal fluid (aCSF). The cutting aCSF contained the following components (in mM): 110 C₅H₁₄NClO, 2.5 KCl, 0.5 CaCl₂, 7 MgCl₂, 1.3 NaH₂PO₄, 25 NaCO₃, 25 glucose (saturated with 95 O₂ and 5% CO₂). Following perfusion, the brain was carefully dissected and sliced into 300 μm thick coronal sections by a vibratome (Leica VT 1200 s) in cutting solution. Coronal slices containing the mPFC and NAc were collected

for recording. These slices were incubated in recording aCSF at 37 °C for 30 min, followed by an additional 30 min at room temperature. The recording aCSF contained the following components (in mM): 125 NaCl, 2.5 KCl, 2 CaCl₂, 1.3 MgCl₂, 1.3 NaH₂PO₄, 25 NaCO₃, 10 glucose. Subsequently, the slices were transferred to a recording chamber and continuously perfused with recording aCSF at a rate of 2 mL/min. Neurons were visualized by a microscope (BXWI51, Olympus) equipped with infrared-differential interference contrast and an infrared camera (IR-1000), and the fluorescence was imaged with U-HGLGPS (Olympus).

Electrophysiology patch-clamp recording

Whole-cell patch-clamp recordings were performed as described previously³⁶. Pipettes were produced by a micropipette puller (Narishige Inc., Japan), and the pipette resistance was controlled between 3 and 5 MΩ. The intracellular pipette solution contained the following components: 115 mM K-methylsulphate, 20 mM NaCl, 1.5 mM MgCl₂, 10 mM HEPES(K), 10 mM BAPTA-tetrapotassium, 1 mg/mL ATP, 0.1 mg/mL GTP, and 1.5 mg/mL sodium phosphocreatine, with a pH of 7.4. Spontaneous and miniature excitatory postsynaptic currents (sEPSCs and mEPSCs) were recorded by using the whole-cell voltage-clamp recordings with an EPC10/2 amplifier controlled by Patchmaster software (HEKA Elektronik, Germany). VTA^{DA} neurons and mPFC cortical neurons were identified by cell-specific expression of EGFP/mCherry, and their AP firing were recorded under current-clamp model in whole-cell configuration. Series conductance and membrane conductance were used to monitor the seal condition during patch-clamp recordings. Signals were sampled at 20 kHz and low-pass filtered at 2.9 kHz. Pharmacological compounds, such as CNO (5 μM), D2R agonist quinpirole (50 nM), D2R antagonist haloperidol (50 nM), were delivered by a gravity-fed perfusion system (MPS-2, Yibo Inc., Wuhan, China). For optogenetic activation of ChR2-expressing neurons/terminals, a blue light pulse was emitted from a collimated light-emitting diode (473 nm) driven by a T-Cube LED Driver (Beijing Viasho Technology Co., Ltd, China) under the control of Pulse software (HEKA Elektronik, Germany). All recordings were conducted at room temperature, and off-line data analysis was performed by Igor software (Wavemetrics).

Amperometric DA recording in brain slices

Amperometric DA recordings in slices were conducted as described in previous studies^{30,33}. CFEs with a diameter of 7 μm and a sensor tip of ~200 μm were employed to measure DA release in the NAc and mPFC. The exposed tip of the CFE was completely inserted into the subsurface of the slice at an angle of ~30°. An EPC10/2 amplifier, controlled by Pulse software (HEKA Electronic, Germany), applied a holding potential of 780 mV to the electrode. Single electrical field stimulus pulses (0.2 ms, 0.6 mA) were delivered through a bipolar platinum electrode (150 μm in diameter) using a Grass S88K stimulator (Astro-Med). In chemogenetic experiments, DA release was triggered by treating the slice with CNO (5 μM) for 10 s. The amperometric current (*I*_{amp}) was low-pass filtered at 100 Hz and digitized at a rate of 3.13 kHz. Off-line data analysis was performed using Igor software (WaveMetric). The paired-pulse ratio was calculated as the ratio of second peak amplitude divided by the first peak amplitude.

Amperometric DA recording in vivo

Amperometric DA recording in the mPFC in vivo was performed following the protocols described in previous studies^{33,36}. Briefly, mice were anesthetized with urethane (1.5 g/kg, i.p.) and secured on a stereotaxic instrument (Narishige, Tokyo, Japan). Body temperature was maintained at 37 °C using a heating pad (KEL-2000, Nanjing, China). A recording carbon fiber electrode with a diameter of 7 μm was implanted in the mPFC at the following coordinates (in mm): AP + 2.8, ML ± 0.5, DV −1.7. An Ag/AgCl reference electrode was placed in the contralateral cortex. A bipolar stimulating electrode was implanted in

the medial forebrain bundle (AP -2.1 , ML ± 1.1 , DV -4.5). Electrical stimulation was delivered as a train of biphasic square-wave pulses (0.6 mA, 1 ms duration) using an isolator (A395, WPI, USA). The carbon fiber electrode was clamped at a potential of 780 mV using an EPC10/2 amplifier controlled by Pulse software (HEKA Electronic, Germany). The amperometric signal (I_{amp}) was low-pass-filtered at 50 Hz and digitized at a rate of 3.13 kHz. Off-line data analysis was performed using Igor software (WaveMetrics).

RNA extraction and qRT-PCR

Total RNA was extracted from peripheral blood using the PAXgene Blood RNA Kit (BD Biosciences, USA) following the manufacturer's instructions. The extracted RNA was then reverse transcribed using the Reverse Transcriptase M-MLV kit (TaKaRa, Japan). Quantitative reverse transcription PCR (qRT-PCR) was performed using the SYBR Premix Ex Taq II kit (TaKaRa, Japan) on a Bio-Rad CFX96 detection instrument (Bio-Rad, USA). The primer sequences for *SYT11* used in this study were AGCTTTGACCGCTTCTCTCG (forward) and CCTCTGCTGATGCACTTCTGG (reverse).

RNA-sequencing data analysis

Total RNA was extracted from the mPFC of adult (3 months old) male mice using Trizol reagent (Invitrogen, USA). After quality control of the RNA samples using the NanoDrop 2000 and Agilent 2100 (Agilent Technologies, USA), the quantified RNA samples were used for library preparation. Sequencing was carried out on an Illumina NovaSeq 6000 platform (Novogene Bioinformatics Institute, China) using the PE150 mode. The RNA-Seq data were mapped to the whole mouse genome sequence. Differential expression analysis was performed to compare control *vs* Syt11 cKO or control virus *vs* chemogenetic manipulated mice. Genes with a fold change >1.5 and a P -value <0.05 were considered as differentially expressed genes (DEGs) and visualized using a volcano plot. Gene ontology (GO) analysis of the DEGs was performed using the cluster Profiler R package, with default parameters for the categories of Cellular Component and Biological Process of GO terms. GO terms with a P -value <0.05 were considered as enriched GO terms.

Protein preparation and western blotting

Western blotting was performed following previously established protocols^{27,30} to assess protein expression. Mice were anesthetized and perfused with ice-cold sectioning aCSF to obtain brain slices (300 μ m thick). The midbrain was meticulously dissected from the brain slices under a dissecting microscope, followed by homogenization in ice-cold buffer composed of 20 mM HEPES at pH 7.4, 100 mM KCl, 2 mM EDTA, 1% NP40, 1 mM PMSF, and 2% protease inhibitor cocktail (P8340, Sigma). The homogenates were then centrifuged at 16,000 g for 15 min at 4 °C, and the supernatants were collected and denatured in sampling buffer. Proteins were separated by electrophoresis and transferred onto nitrocellulose filter membranes. The membranes were blocked by incubating in a phosphate-balanced saline (PBS) solution containing 0.1% Tween-20 (v/v) and 5% non-fat dried milk (w/v) for 1 h. After washing with PBST (PBS containing 0.1% Tween-20), the blots were incubated overnight at 4 °C with primary antibodies diluted in PBST containing 2% bovine serum albumin (BSA). The primary antibodies used in the present study were rabbit anti-tyrosine hydroxylase (TH) (AB152, Millipore, 1:1000), rabbit anti-Syt11 (270003, Synaptic Systems, 1:1000), and rabbit anti-GAPDH (ab9485, Abcam, 1:1000). Subsequently, the membranes were washed with PBST containing 0.05% Tween-20 and incubated with HRP-conjugated fluorescence-labelled secondary antibodies at room temperature for 1 h. The secondary antibodies employed were goat anti-rabbit IgG (149393, Jackson Immuno Research 1:3000) and goat anti-mouse IgG (148774, Jackson Immuno Research, 1:3000). The blots were visualized using the Clarity Western ECL substrate, scanned with the Clix chemical

capture system (Clix Science Instruments Co., Ltd), and quantified with ImageJ (National Institutes of Health).

Immunofluorescence

The mice were anesthetized with avertin and perfused with 0.9% saline followed by 4% paraformaldehyde (PFA, Sigma) in PBS 3 weeks or 6 weeks (virus injection at P0) post-virus injection. The brain was swiftly removed and post-fixed in 4% PFA for 24 h at 4 °C. Following dehydration in 10%, 20%, and 30% sucrose at 4 °C for 3–4 days, a series of coronal sections (30 μ m thick) were sliced using a cryostat microtome system (MEV, SLEE, Germany). The sections were rinsed three times with PBS and then permeabilized with 0.3% Triton X-100 in PBS containing 2% BSA for 8 min at room temperature. After a 1-hour blocking step with 2% BSA in PBS, the sections were incubated with the primary antibodies overnight at 4 °C. The primary antibodies used were rabbit anti-TH (213102; 1:1000), mouse anti-TH (213211; 1:1000), and rabbit anti-Syt11 (270003; 1:500) from Synaptic Systems. After five washes with blocking solution, the samples were incubated with the secondary antibodies at room temperature for 2 h. The secondary antibodies employed were donkey anti-rabbit Alexa488 (2289872; 1:1000), donkey anti-mouse Alexa488 (2229195; 1:1000), donkey anti-rabbit Alexa594 (2266563; 1:1000), donkey anti-mouse Alexa594 (2234977; 1:1000), and donkey anti-rabbit Alexa647 (LC-307589; 1:1000) from Invitrogen. Following five washes in blocking solution and one wash in PBS, the sections were stained with DAPI and mounted on microslides with anti-fade mounting medium. Fluorescence images were captured on a Leica TCS SP8 STED inverted confocal microscope (Leica, Germany). The images were analyzed using ImageJ software (National Institutes of Health, Bethesda, MD) and packaged with Adobe Photoshop (Adobe Systems Inc.).

TIRF imaging

TIRF imaging was performed on an inverted microscope equipped with a 100 \times TIRF objective lens (Nikon ECLIPSE Ti-U; numerical aperture 1.45). Images were captured using an Andor EMCCD camera with NIS-Elements BR software, with an exposure time of 200 ms. Surface D2R fluorescence intensity values were calculated and analyzed using ImageJ software. Both the transfected and non-transfected cells were calculated and the fluorescence intensity of transfected cells were normalized by the non-transfected cells.

Behavioral tests

The procedures for behavioral tests were conducted following the methods described in a previous study³⁶. Mice were transported in their home cage to the testing room 1 h before the tests for environmental habituation. The behaviors of the animals were recorded using an overhead camera and the Anymaze tracking system (Stoelting Inc.), unless otherwise specified. Pharmacological, chemogenetic, and optogenetic manipulations were applied as described below. Dim light (~ 20 lux) was used in the testing room to minimize anxiety in the mice.

Social and social novelty test. This assay was performed using a Plexiglas rectangular box (40 \times 20 \times 22 cm) consisting of three interconnected chambers of equal size. For habituation, the test mouse was placed in the central chamber and allowed to freely explore all three chambers for 10 min. Mice that showed a preference for a specific side chamber were excluded from the test. After habituation, the test mouse was placed in the center chamber with both gates to the side chambers closed. An age- and gender-matched stranger mouse (M1) was introduced in a mesh cage in one side chamber, while a fake mouse (F) was placed in a similar mesh cage in the other side chamber. The test mouse was allowed to freely explore for 10 min after the opening of both gates. The interaction time was measured as the sum of all time intervals the test mouse spent sniffing and approaching the M1 or F

mouse. The social preference index was calculated as the ratio of sniffing time with M1 *versus* M1 + F, as previously described⁷⁸.

In the social novelty test, the same test mouse was placed in the center chamber with both gates to the side chambers closed. The former stranger mouse (M1, familiar mouse in novelty test) remained unchanged, but the fake mouse was replaced by another age- and sex-matched stranger mouse (M2). The test mouse was allowed to freely explore and was monitored for an additional 10 min. The interaction times that the test mouse spent sniffing and approaching the M1 or M2 mouse were analyzed. The arena was thoroughly cleaned with 75% ethanol after each trial, and the mouse was returned to its own home cage.

Social approach test. This test was performed in an open field apparatus (40 × 40 × 40 cm) with a cylindrical mesh cage fixed in the center area. An age- and gender-matched stranger mouse was placed inside the central cage, while the test mouse was placed in the apparatus and allowed to freely explore its surroundings for 30 min. The movement and activity of the mice were monitored using a video tracking system and analyzed with Anymaze software (Stoelting Inc.). The time each mouse sniffing the cylindrical mesh cage or the stranger mice was measured. The apparatus was cleaned with 75% ethanol after each test, and the mouse was returned to its home cage.

Home-cage social test. The test mouse was individually housed and fed for 5 days without changing the padding before the experiment. An age- and sex-matched intruder mouse was introduced into the resident's home cage and allowed to freely explore for 30 min. The time and frequency of contact between the resident and the intruder were monitored using an overhead camera and analyzed with Anymaze software (Stoelting Inc.).

Prepulse inhibition (PPI) test. The PPI test was conducted in a standard sound-attenuated cabinet (Zhongshi technology Inc., Beijing, China). Prior to the test, the device was calibrated and standardized for each mouse. The test mouse was acclimatized to a Plexiglas cylinder with a background noise of -65 dB (white noise) for 5 min. Subsequently, the mouse was exposed to six blocks of seven trial types presented in a pseudorandom order, with an average inter-trial interval of 15 s. The seven trial types included: trial 1, basal startle responses (40-ms 120 dB startle-only pulse, 5 pulses with a 15-s inter-pulse interval); trials 2–6, prepulse tests (three paired-pulse stimuli applied in a random order, with each consisting of a 20-ms prepulse of 72, 76, or 80 dB acoustic stimulus followed by a 120 dB startle stimulus 100 ms after prepulse); and trial 7, 120 dB startle-only, 5 pulses with a 15-s interval. The startle response was measured as the maximum response within the 65-ms sampling window following each set of stimuli. The averaged startle response was used to calculate the percentage inhibition (PPI %) of each type of stimulus, representing the percentage reduction in startle response compared with the startle stimulus.

Locomotion and grooming. Each mouse was placed in the center area of an open field apparatus (40 × 40 × 40 cm) and allowed to freely explore its surroundings. The movement and activity of the mice were tracked and analyzed using an overhead camera and the Anymaze tracking system (Stoelting Inc.). Grooming behaviors, including face-wiping, scratching/rubbing of the head and ears, or whole-body grooming, were quantified over a 15-min period. The average speed, maximum speed, and total travel distance in 15 min were measured to assess locomotor activity. The apparatus was cleaned with 75% ethanol after each test.

Marble burying. Before the test, the home-cage padding was changed to corncob for at least 4 days. The testing mouse was then placed in a

new home cage with fresh corncob padding (5 cm in depth) with 18 clean marbles prearranged in a 3 by 6 grid. The mouse was allowed to bury the marbles for 15 min, and the number of buried marbles was counted immediately after the test. Only marbles that were at least 2/3 covered with corncob padding were considered as buried.

Food-induced T-maze. The mice were food-deprived for 24 h before the test. The T-maze consisted of a start arm and two identical goal arms (30 × 10 × 20 cm for each arm). A 2-g pellet of regular chow was placed in the corner of one of the goal arms. The test mouse was habituated in the start arm for 90 s. After opening the gate in the start arm, the mouse was allowed to freely explore the T-maze. When the test mouse entered the goal arm and found the food, the gate in the goal arm was closed. The mouse was returned to its home cage after consuming the food, and 10 min later, the trial was repeated but without any food in the goal arm. The time taken by the mouse to reach the goal arm was recorded to assess short-term memory. To prevent discrimination of the goal arm based on odor, the entire apparatus was thoroughly cleaned with 75% ethanol before and after each trial.

Y-maze. The test mouse was transferred into the central area of a Y-maze apparatus consisting of three dark gray arms (L: 30 cm, W: 8 cm, H: 15 cm for each arm). The mouse was allowed to freely explore all three arms for 10 min, and its movements were monitored using an overhead camera and the Anymaze tracking system (Stoelting Inc.). The number of entries into the arms and the number of alternations were quantified. The ratio of correct alternations to the total number of new arm entries was used to determine short-term memory. Spontaneous alternation was calculated as: SPA% = (number of alternations / [total number of arm entries - 2]) × 100.

Behavioral pharmacology

Drugs were administered through a bilateral stainless-steel inner cannula (RWD, China) connected to a dummy micro-tube, controlled by a micro-syringe pump. The D2 agonist quinpirole (QP, 1 μg/μl, 0.2 μl/side), D2 antagonist haloperidol (Halo, 50 μM, 0.2 μl/side), or saline were locally infused at a rate of 100 nl/min. All drugs were prepared in buffered saline. The internal cannula was withdrawn 2 min after infusion, and social testing was conducted 10 min after drug administration.

Optogenetic manipulation

Behavioral testing was performed at least 3 weeks after virus injection to ensure the expression of ChR2 *in vivo*. Optical fiber implants were connected to a patch cable using a ceramic sleeve (RWD, China), which was further connected to a commutator (Newdoon Technology Co., Ltd, China) via an FC/PC adapter to allow unrestricted movement of the test mouse. Bursts of 473-nm light (5-ms, 8 pulses at 30 Hz) were delivered once every 5 s at an output power of 10 mW, controlled by an Intelligent Light System (Newdoon Technology Co., Ltd, China).

Chemogenetic manipulation

The TH-Cre virus and Cre-dependent chemogenetic activation virus (DIO-hM3Dq) were co-injected into the VTA of P0 C57 mice or mice aged 3 weeks. The ligand clozapine-N-oxide (CNO) from Sigma-Aldrich (St. Louis, MO) was dissolved in saline. For electrophysiological and electrochemical slice recordings, CNO (5 μM) was delivered using a gravity-fed perfusion system (MPS-2, Yibo Inc., Wuhan, China). Acute chemogenetic activation *in vivo* was applied three weeks after virus injection, and behavioral tests were conducted 20 min after CNO administration (0.5 mg/kg, *i.p.*). To assess the long-lasting effect of repetitive chemogenetic activation *in vivo*, systemic treatment with CNO (0.5 mg/kg, *i.p.* injection) was administered every second day between P7 and P14, and behavioral tests were conducted 4–6 weeks after the CNO treatment or during adulthood as indicated.

Statistics and reproducibility

All experiments were performed with side-by-side controls and in a random order, and were replicated at least three times. Sample sizes were not predetermined using statistical methods, but were consistent with those reported in similar studies. No samples or animals that yielded successful measurements were excluded from the analysis. To preprocess the three RNA-Sequencing datasets of human brain tissues (LIBD, CMC, and HBCC), we normalized raw counts to counts per million (CPM) by dividing each count with the total count of the corresponding samples in each dataset, and then multiplying by one million to account for differences in sequencing depth across samples. To mitigate the effects of low expression values, we performed a log₂ transformation of the CPM values by calculating the base-2 logarithm of each value. All statistical tests were performed using GraphPad Prism version 9.0 (GraphPad Software Inc.), R version 4.1 (<https://cran.r-project.org/>), or SPSS version 18.0. The Shapiro-Wilk test was used to test the normality of data, and Levene's test was used to assess the equality of variance. Statistical comparisons were conducted using the Wilcoxon–Mann-Whitney non-parametric test, Pearson correlation analysis, paired Student's t-test, one-way ANOVA, or two-way ANOVA (followed by Bonferroni's or Tukey's multiple comparisons were used to make comparisons) as indicated. In all between-group comparisons, the type I error rate was set at 0.05 ($\alpha = 0.05$, two-tailed). Significant differences were accepted at $P < 0.05$. Data are shown as box-and-whisker plots or mean \pm s.e.m. as indicated, and the numbers of cells, slices, mice, or human samples analyzed are presented in the figures.

Reporting summary

Further information on research design is available in the Nature Portfolio Reporting Summary linked to this article.

Data availability

All data presented in this study are either included in this article and its Supplemental Information or are available upon request to the corresponding author. The RNA-Seq data generated in this study have been deposited in Sequence Read Archive (SRA) under accession code [PRJNA1162940](https://www.ncbi.nlm.nih.gov/sra/PRJNA1162940). Source data are provided with this paper.

References

- Marder, S. R. & Cannon, T. D. Schizophrenia. *N. Eng. J. Med.* **381**, 1753–1761 (2019).
- Kahn, R. S. et al. Schizophrenia. *Nat. Rev. Dis. Prim.* **1**, 15067 (2015).
- Fish, K. N. et al. Altered Parvalbumin Basket Cell Terminals in the Cortical Visuospatial Working Memory Network in Schizophrenia. *Biol. Psychiatry* **90**, 47–57 (2021).
- Howes, O. D., McCutcheon, R., Owen, M. J. & Murray, R. M. The role of genes, stress, and dopamine in the development of schizophrenia. *Biol. Psychiatry* **81**, 9–20 (2017).
- Stroup, T. S. & Gray, N. Management of common adverse effects of antipsychotic medications. *World Psychiatry* **17**, 341–356 (2018).
- Smeland, O. B., Frei, O., Dale, A. M. & Andreassen, O. A. The polygenic architecture of schizophrenia - rethinking pathogenesis and nosology. *Nat. Rev. Neurol.* **16**, 366–379 (2020).
- Goff, D. C. The Pharmacologic Treatment of Schizophrenia—2021. *JAMA* **325**, 175–176 (2021).
- Grace, A. A. Dysregulation of the dopamine system in the pathophysiology of schizophrenia and depression. *Nat. Rev. Neurosci.* **17**, 524–532 (2016).
- Laruelle, M., Abi-Dargham, A., Gil, R., Kegeles, L. & Innis, R. Increased dopamine transmission in schizophrenia: relationship to illness phases. *Biol. Psychiatry* **46**, 56–72 (1999).
- Zhu, Y., Wienecke, C. F. R., Nachtrab, G. & Chen, X. A thalamic input to the nucleus accumbens mediates opiate dependence. *Nature* **530**, 219–222 (2016).
- Zhu, X. et al. Thalamic reticular nucleus impairments and abnormal prefrontal control of dopamine system in a developmental model of schizophrenia: prevention by N-acetylcysteine. *Mol. Psychiatry* **26**, 7679–7689 (2021).
- Howes, O. D. et al. Dopamine synthesis capacity before onset of psychosis: a prospective [18F]-DOPA PET imaging study. *Am. J. Psychiatry* **168**, 1311–1317 (2011).
- Zhu, X. & Grace, A. A. Sex- and exposure age-dependent effects of adolescent stress on ventral tegmental area dopamine system and its afferent regulators. *Mol. Psychiatry* **28**, 611–624 (2023).
- McCutcheon, R. A., Krystal, J. H. & Howes, O. D. Dopamine and glutamate in schizophrenia: biology, symptoms and treatment. *World Psychiatry* **19**, 15–33 (2020).
- McCutcheon, R. A., Abi-Dargham, A. & Howes, O. D. Schizophrenia, Dopamine and the Striatum: From Biology to Symptoms. *Trends Neurosci.* **42**, 205–220 (2019).
- Slifstein, M. et al. Deficits in prefrontal cortical and extrastriatal dopamine release in schizophrenia: a positron emission tomographic functional magnetic resonance imaging study. *JAMA Psychiatry* **72**, 316–324 (2015).
- Frankle, W. G., Himes, M., Mason, N. S., Mathis, C. A. & Narendran, R. Prefrontal and Striatal Dopamine Release Are Inversely Correlated in Schizophrenia. *Biol. Psychiatry* **92**, 791–799 (2022).
- Mukherjee, A., Carvalho, F., Eliez, S. & Caroni, P. Long-Lasting rescue of network and cognitive dysfunction in a genetic schizophrenia model. *Cell* **178**, 1387–1402 (2019).
- Abi-Dargham, A. A Dual Hit Model for Dopamine in Schizophrenia. *Biol. Psychiatry* **81**, 2–4 (2017).
- Wong, A. H. & Josselyn, S. A. Caution When Diagnosing Your Mouse With Schizophrenia: The Use and Misuse of Model Animals for Understanding Psychiatric Disorders. *Biol. Psychiatry* **79**, 32–38 (2016).
- Tromp, A., Mowry, B. & Giacomotto, J. Neurexins in autism and schizophrenia—a review of patient mutations, mouse models and potential future directions. *Mol. Psychiatry* **26**, 747–760 (2021).
- Uliana, D. L., Gomes, F. V. & Grace, A. A. Update on current animal models for schizophrenia: are they still useful? *Curr. Opin. Psychiatry* **36**, 172–178 (2023).
- Inoue, S. et al. Synaptotagmin XI as a candidate gene for susceptibility to schizophrenia. *Am. J. Med Genet B Neuropsychiatr. Genet* **144B**, 332–340 (2007).
- Brzustowicz, L. M., Hodgkinson, K. A., Chow, E. W., Honer, W. G. & Bassett, A. S. Location of a major susceptibility locus for familial schizophrenia on chromosome 1q21-q22. *Science* **288**, 678–682 (2000).
- Pang, Z. P. & Südhof, T. C. Cell biology of Ca²⁺-triggered exocytosis. *Curr. Opin. Cell Biol.* **22**, 496–505 (2010).
- von Poser, C., Ichtchenko, K., Shao, X., Rizo, J. & Südhof, T. C. The evolutionary pressure to inactivate. A subclass of synaptotagmins with an amino acid substitution that abolishes Ca²⁺ binding. *J. Biol. Chem.* **272**, 14314–14319 (1997).
- Wang, C. et al. Synaptotagmin-11 inhibits clathrin-mediated and bulk endocytosis. *EMBO Rep.* **17**, 47–63 (2016).
- Wu, X., Hu, S., Kang, X. & Wang, C. Synaptotagmins: beyond pre-synaptic neurotransmitter release. *Neuroscientist* **26**, 9–15 (2020).
- Chen, Y. et al. Synaptotagmin-1 is a bidirectional Ca²⁺ sensor for neuronal endocytosis. *Proc. Natl Acad. Sci. USA* **119**, e2111051119 (2022).
- Wang, C. et al. Synaptotagmin-11 is a critical mediator of parkin-linked neurotoxicity and Parkinson's disease-like pathology. *Nat. Commun.* **9**, 81 (2018).
- Hoffman, G. E. et al. CommonMind Consortium provides transcriptomic and epigenomic data for Schizophrenia and Bipolar Disorder. *Sci. Data* **6**, 180 (2019).

32. Xu, D. et al. WDR62-deficiency Causes Autism-like Behaviors Independent of Microcephaly in Mice. *Neurosci. Bull.* **39**, 1333–1347 (2023).
33. Kang, X. et al. Dopamine release from transplanted neural stem cells in Parkinsonian rat striatum in vivo. *Proc. Natl Acad. Sci. USA* **111**, 15804–15809 (2014).
34. Li, Y. et al. Identification of two functionally distinct endosomal recycling pathways for dopamine D(2) receptor. *J. Neurosci.: Off. J. Soc. Neurosci.* **32**, 7178–7190 (2012).
35. Gunaydin, L. A. et al. Natural neural projection dynamics underlying social behavior. *Cell* **157**, 1535–1551 (2014).
36. Li, M. et al. Impaired D2 receptor-dependent dopaminergic transmission in prefrontal cortex of awake mouse model of Parkinson's disease. *Brain* **142**, 3099–3115 (2019).
37. Harvey, I. et al. Reduction of cortical volume in schizophrenia on magnetic resonance imaging. *Psychological Med.* **23**, 591–604 (1993).
38. Brugger, S. P. & Howes, O. D. Heterogeneity and Homogeneity of Regional Brain Structure in Schizophrenia: A Meta-analysis. *JAMA Psychiatry* **74**, 1104–1111 (2017).
39. Onwordi, E. C., et al. Synaptic density marker SV2A is reduced in schizophrenia patients and unaffected by antipsychotics in rats. *Nat Commun* **11**, 246 (2020).
40. Pakkenberg, B. Post-mortem study of chronic schizophrenic brains. *Br. J. Psychiatry.: J. Ment. Sci.* **151**, 744–752 (1987).
41. Osimo, E. F., Beck, K., Reis Marques, T. & Howes, O. D. Synaptic loss in schizophrenia: a meta-analysis and systematic review of synaptic protein and mRNA measures. *Mol. Psychiatry* **24**, 549–561 (2019).
42. Howes, O. D. & Onwordi, E. C. The synaptic hypothesis of schizophrenia version III: a master mechanism. *Molecular psychiatry* **28**, 1843–1856 (2023).
43. Rolls, E. T. Attractor cortical neurodynamics, schizophrenia, and depression. *Transl. Psychiatry* **11**, 215 (2021).
44. Borglum, A. D. et al. Dopa decarboxylase genotypes may influence age at onset of schizophrenia. *Mol. Psychiatry* **6**, 712–717 (2001).
45. Cai, H. Q. et al. Altered levels of immune cell adhesion molecules are associated with memory impairment in schizophrenia and healthy controls. *Brain, Behav., Immun.* **89**, 200–208 (2020).
46. Harrison, P. J. & Law, A. J. Neuregulin 1 and schizophrenia: genetics, gene expression, and neurobiology. *Biol. Psychiatry* **60**, 132–140 (2006).
47. Manago, F. et al. Genetic Disruption of Arc/Arg3.1 in Mice Causes Alterations in Dopamine and Neurobehavioral Phenotypes Related to Schizophrenia. *Cell Rep.* **16**, 2116–2128 (2016).
48. Simpson, E. H., Gallo, E. F., Balsam, P. D., Javitch, J. A. & Kellendonk, C. How changes in dopamine D2 receptor levels alter striatal circuit function and motivation. *Mol. Psychiatry* **27**, 436–444 (2022).
49. Missale, C., Nash, S. R., Robinson, S. W., Jaber, M. & Caron, M. G. Dopamine receptors: from structure to function. *Physiol. Rev.* **78**, 189–225 (1998).
50. McCutcheon, R. A., Reis Marques, T. & Howes, O. D. Schizophrenia-An Overview. *JAMA Psychiatry* **77**, 201–210 (2020).
51. Skene, N. G. et al. Genetic identification of brain cell types underlying schizophrenia. *Nat. Genet* **50**, 825–833 (2018).
52. Rein, B., Ma, K. & Yan, Z. A standardized social preference protocol for measuring social deficits in mouse models of autism. *Nat. Protoc.* **15**, 3464–3477 (2020).
53. Huang, Y. et al. ZFP804A mutant mice display sex-dependent schizophrenia-like behaviors. *Mol. Psychiatry* **26**, 2514–2532 (2021).
54. Assous, M. et al. Differential processing of thalamic information via distinct striatal interneuron circuits. *Nat. Commun.* **8**, 15860 (2017).
55. Shimojo, M. et al. Synaptotagmin-11 mediates a vesicle trafficking pathway that is essential for development and synaptic plasticity. *Genes Dev.* **33**, 365–376 (2019).
56. Du, C. et al. Synaptotagmin-11 inhibits cytokine secretion and phagocytosis in microglia. *Glia* **65**, 1656–1667 (2017).
57. Mittelstaedt, T. et al. Differential mRNA expression patterns of the synaptotagmin gene family in the rodent brain. *J. Comp. Neurol.* **512**, 514–528 (2009).
58. Maia, T. V. & Frank, M. J. An Integrative Perspective on the Role of Dopamine in Schizophrenia. *Biol. Psychiatry* **81**, 52–66 (2017).
59. Abi-Dargham, A. et al. Increased baseline occupancy of D2 receptors by dopamine in schizophrenia. *Proc. Natl Acad. Sci. USA* **97**, 8104–8109 (2000).
60. Howes, O. D. & Shatalina, E. Integrating the Neurodevelopmental and Dopamine Hypotheses of Schizophrenia and the Role of Cortical Excitation-Inhibition Balance. *Biol. Psychiatry* **92**, 501–513 (2022).
61. Lisman, J. E. et al. Circuit-based framework for understanding neurotransmitter and risk gene interactions in schizophrenia. *Trends Neurosci.* **31**, 234–242 (2008).
62. Provenzano, F. A. et al. Hippocampal Pathology in Clinical High-Risk Patients and the Onset of Schizophrenia. *Biol. Psychiatry* **87**, 234–242 (2020).
63. Weinstein, J. J. et al. Pathway-Specific Dopamine Abnormalities in Schizophrenia. *Biol. Psychiatry* **81**, 31–42 (2017).
64. Bariselli, S. et al. SHANK3 controls maturation of social reward circuits in the VTA. *Nat. Neurosci.* **19**, 926–934 (2016).
65. Brumback, A. C. et al. Identifying specific prefrontal neurons that contribute to autism-associated abnormalities in physiology and social behavior. *Mol. Psychiatry* **23**, 2078–2089 (2018).
66. Tseng, K.-Y. & O'Donnell, P. Dopamine modulation of prefrontal cortical interneurons changes during adolescence. *Cereb. Cortex* **17**, 1235–1240 (2007).
67. Urs, N. M. et al. Distinct cortical and striatal actions of a β -arrestin-biased dopamine D2 receptor ligand reveal unique antipsychotic-like properties. *Proc. Natl Acad. Sci. USA* **113**, E8178–E8186 (2016).
68. Gee, S. et al. Synaptic activity unmasks dopamine D2 receptor modulation of a specific class of layer V pyramidal neurons in prefrontal cortex. *J. Neurosci.* **32**, 4959–4971 (2012).
69. Robinson, S. E. & Sohal, V. S. Dopamine D2 Receptors Modulate Pyramidal Neurons in Mouse Medial Prefrontal Cortex through a Stimulatory G-Protein Pathway. *J. Neurosci.* **37**, 10063–10073 (2017).
70. Clarkson, R. L., Liptak, A. T., Gee, S. M., Sohal, V. S. & Bender, K. J. D3 Receptors Regulate Excitability in a Unique Class of Prefrontal Pyramidal Cells. *J. Neurosci.* **37**, 5846–5860 (2017).
71. Wang, L. et al. Cocaine induces locomotor sensitization through a dopamine-dependent VTA-mPFC-FrA cortico-cortical pathway in male mice. *Nat. Commun.* **14**, 1568 (2023).
72. Moya, N. A. et al. The effect of selective nigrostriatal dopamine excess on behaviors linked to the cognitive and negative symptoms of schizophrenia. *Neuropsychopharmacology* **48**, 690–699 (2023).
73. Simpson, E. H. & Kellendonk, C. Insights About Striatal Circuit Function and Schizophrenia From a Mouse Model of Dopamine D Receptor Upregulation. *Biol. Psychiatry* **81**, 21–30 (2017).
74. Wu, S., Gao, C., Han, F. & Cheng, H. Histamine H1 Receptor in Basal Forebrain Cholinergic Circuit: A Novel Target for the Negative Symptoms of Schizophrenia? *Neurosci. Bull.* **38**, 558–560 (2022).
75. Gill, K. M., Cook, J. M., Poe, M. M. & Grace, A. A. Prior antipsychotic drug treatment prevents response to novel antipsychotic agent in the methylazoxymethanol acetate model of schizophrenia. *Schizophr. Bull.* **40**, 341–350 (2014).
76. Valenti, O. & Grace, A. A. Antipsychotic drug-induced increases in ventral tegmental area dopamine neuron population activity via activation of the nucleus accumbens-ventral pallidum pathway. *Int J. Neuropsychopharmacol.* **13**, 845–860 (2010).
77. Wei, C. et al. Response dynamics of midbrain dopamine neurons and serotonin neurons to heroin, nicotine, cocaine, and MDMA. *Cell Discov.* **4**, 60 (2018).

78. Dong, Z., et al. CUL3 deficiency causes social deficits and anxiety-like behaviors by impairing excitation-inhibition balance through the promotion of cap-dependent translation. *Neuron* **105**, 475–490 (2020).

Acknowledgements

We thank Drs. Han Xu (Zhejiang University, China) for discussion and comments, Minmin Luo (National Institute of Biological Sciences, China) for DAT-Cre mice, Xianghui Zhao (Fourth Military Medical University, China) for discussion and prepulse inhibition test, Ying Hao (Core Facilities Sharing Platform, Xi'an Jiaotong University, China) for assistance with confocal imaging, Enle Wang (High School Affiliated to Xi'an Jiaotong University, China) for art work, and Iain C. Bruce (Peking University, China) for reading the manuscript. This work was supported by the National Natural Science Foundation of China (32171233 to C.W., 81901308 to H.X., 81974203 to X.K., 82222031 to F.G., 32300819 to Y.C., and 32000704 to Q.S.), the Natural Science Foundation of Shaanxi Province of China (2023-ZDLSF-23, 2021TD-37, and 2019JC-07 to C.W.; 2020JQ-029 to Q.S.; 2023-JC-QN-0236 to N.D.; 2024JC-YBMS-146 to H.X.; JC-YBQN-0172 to C.Z.; and 2024RS-CXTD-80 to F.G.), the Sichuan Science and Technology Program (2022YFS0615 and 2024ZYD0077 to X.K.), the China Postdoctoral Science Foundation (2018M640972 to Q.S.; 2022M712543 to N.D.; 2024M752559, 2024T170724, and GZC20232111 to Y.C.), and the Shaanxi Postdoc Funding (2023BSHTBZZ15 to H.X., 2023BSHYDZZ39 to Y.C., and 2023BSHEDZZ67 to C.Z.). Figure 2r and Supplemental Fig. 19 are created at BioRender.com with the publication license.

Author contributions

C.W., X.K., H.X. and F.G. conceived the study and designed the experiments with the help of S.Z. and Q.Q. Y.C., Y.G., B.W., A.W., N.D., Y. J., X.L., L.Z., F.Z., T.T., Z.J., F.M., Y.Z., J.Y., Y.Y., H. Wang, H. Wu, H.L., C.Z., X.D., J.H., X.W., S.H., A.Z., Z.L., X.C., Y.Q., and Q.S. performed the experiments and analyses. C.W., X.K., H.X., F.G., and Y.C. wrote the manuscript. All authors reviewed the manuscript and approved its submission.

Competing interests

The authors declare no competing interests.

Additional information

Supplementary information The online version contains supplementary material available at <https://doi.org/10.1038/s41467-024-54604-4>.

Correspondence and requests for materials should be addressed to Fanglin Guan, Huadong Xu, Xinjiang Kang or Changhe Wang.

Peer review information *Nature Communications* thanks the anonymous reviewers for their contribution to the peer review of this work. A peer review file is available.

Reprints and permissions information is available at <http://www.nature.com/reprints>

Publisher's note Springer Nature remains neutral with regard to jurisdictional claims in published maps and institutional affiliations.

Open Access This article is licensed under a Creative Commons Attribution-NonCommercial-NoDerivatives 4.0 International License, which permits any non-commercial use, sharing, distribution and reproduction in any medium or format, as long as you give appropriate credit to the original author(s) and the source, provide a link to the Creative Commons licence, and indicate if you modified the licensed material. You do not have permission under this licence to share adapted material derived from this article or parts of it. The images or other third party material in this article are included in the article's Creative Commons licence, unless indicated otherwise in a credit line to the material. If material is not included in the article's Creative Commons licence and your intended use is not permitted by statutory regulation or exceeds the permitted use, you will need to obtain permission directly from the copyright holder. To view a copy of this licence, visit <http://creativecommons.org/licenses/by-nc-nd/4.0/>.

© The Author(s) 2024

¹Department of Neurology, the Second Affiliated Hospital, Neuroscience Research Center, Key Laboratory of Biomedical Information Engineering of Ministry of Education, School of Life Science and Technology, Xi'an Jiaotong University, Xi'an 710049, China. ²Department of Neurosurgery, the Affiliated Hospital of Southwest Medical University, Luzhou Sichuan 646000, China. ³Key Laboratory of Medical Electrophysiology, Ministry of Education of China, Collaborative Innovation Center for Prevention and Treatment of Cardiovascular Disease, and the Institute of Cardiovascular Research, Southwest Medical University, Luzhou 646000, China. ⁴College of Life Sciences, Liaocheng University, Liaocheng 252059, China. ⁵Key Laboratory of National Health Commission for Forensic Sciences, College of Medicine & Forensics, Xi'an Jiaotong University, Xi'an 710061, China. ⁶Center for Translational Medicine, the First Affiliated Hospital of Xi'an Jiaotong University, Xi'an 710061, China. ⁷Oujiang Laboratory (Zhejiang Lab for Regenerative Medicine, Vision and Brain Health), Institute of Aging, Key Laboratory of Alzheimer's Disease of Zhejiang Province, Zhejiang Provincial Clinical Research Center for Mental Disorders, The Affiliated Wenzhou Kangning Hospital, Wenzhou Medical University, Wenzhou 325035, China. ⁸Department of Neurology, the First Affiliated Hospital of Xi'an Jiaotong University, Xi'an 710061, China. ⁹Department of Psychology, Chengwu People's Hospital, Heze 274200, China. ¹⁰These authors contributed equally: Yang Chen, Yuhao Gu, Bianbian Wang, Anqi Wei. ✉ e-mail: fanglingguan@163.com; hdxu@pku.edu.cn; kxj335@163.com; changhewang@xjtu.edu.cn